RSC Advances

REVIEW

View Article Online
View Journal | View Issue

Cite this: *RSC Adv.*, 2026, **16**, 29368

Hierarchical pore engineering in waste-derived carbons for supercapacitors: bridging the performance gap from three-electrode evaluation to practical two-electrode devices

Mustapha Balarabe Idris, * Bhekie B. Mamba and Fuku Xolile

Supercapacitors based on waste-derived porous carbons have attracted significant attention due to their low cost, sustainability, and tunable pore structures. However, a persistent discrepancy remains between the high capacitance values reported in three-electrode (half-cell) configurations and the significantly lower performance observed in practical two-electrode devices. This gap is frequently overlooked, leading to overestimation of material performance and limiting the translation of laboratory-scale results into real applications. This review critically examines recent advances in hierarchical pore engineering of waste-derived carbons with a specific focus on understanding and bridging the performance gap between intrinsic material properties and device-level behaviour. We first analyse the fundamental differences between three-electrode and two-electrode evaluation systems, highlighting the origins of performance inflation that arise from low mass loading, restricted voltage windows, electrolyte effects, and the neglect of internal resistance. A quantitative and mechanistic framework is then established to explain the translation of capacitance from single-electrode to full-cell configurations. Building on this, structure–performance relationships are systematically evaluated across multiple studies to identify why materials with ultrahigh surface areas (>2000 m^2 g^{-1}) often fail to deliver superior device performance. Particular attention is given to the roles of pore accessibility, ion transport limitations, electrolyte-pore matching, and the trade-off between porosity and electrical conductivity. The effectiveness of hierarchical pore architectures and heteroatom doping is critically reassessed, distinguishing genuine performance enhancements from overstated effects. Finally, design principles for developing device-relevant carbon electrodes are proposed, emphasising accessible porosity, optimised pore connectivity, and realistic testing conditions. Practical challenges related to scalability, reproducibility, and environmental impact are also discussed. This review provides a comprehensive framework for transitioning from inflated laboratory metrics to reliable, high-performance supercapacitor devices based on waste-derived carbons.

Received 19th April 2026
Accepted 13th May 2026

DOI: 10.1039/d6ra03341e

rsc.li/rsc-advances

1. Introduction

Supercapacitors have emerged as promising candidates for various applications, including portable electronics, hybrid electric vehicles, and grid-scale energy storage, owing to their high power density, rapid charge/discharge rates, and extended cycle life.[1,2] This makes them attractive alternatives or complements to batteries, particularly where high power delivery and long-term stability are critical. Their performance critically hinges on the electrode materials, which are expected to possess attributes such as a large accessible surface area, high electrical conductivity, and stable electrochemical interfaces to facilitate efficient charge accumulation and accelerate redox reactions.[3–5] Among the various materials investigated, porous carbon has garnered significant attention as an electrode material for electric double-layer capacitors due to its high specific surface area and tunable pore architecture.[6] Of special interest, the utilisation of waste-derived carbon precursors offers an economical and eco-friendly pathway for producing these critical materials, simultaneously addressing waste management challenges and resource scarcity.[7] This approach transforms discarded industrial plastic and biomass waste into value-added porous carbon materials for energy storage, aligning with the principles of sustainable development and the circular economy.[8,9] Nevertheless, despite the inherent advantages of biomass-derived carbon, challenges persist in optimising its pore structure and surface chemistry to achieve high energy densities comparable to those of batteries while maintaining

Institute for Nanotechnology and Water Sustainability, College of Science, Engineering and Technology, University of South Africa, Florida Science Campus, 1710, South Africa. E-mail: idrisbm@unisa.ac.za

the characteristic high power densities of supercapacitors.[10] This necessitates hierarchical pore engineering to enhance ion transport kinetics and maximise the electrochemically active surface area within the carbon matrix. Indeed, several recent reviews have comprehensively discussed the synthesis, activation strategies, heteroatom doping, and electrochemical performance of waste-derived porous carbons for supercapacitor applications.[11–15] These studies primarily focus on precursor selection, pore-engineering approaches, and the maximisation of gravimetric capacitance values under laboratory-scale testing conditions. However, despite the rapid growth of the field, a critical issue of large discrepancy between the exceptionally high capacitance values reported in three-electrode configurations and the substantially lower performance achieved in practical two-electrode devices remains insufficiently addressed. Besides, the performance metrics for waste-derived carbons are largely based on gravimetric measurements conducted under controlled laboratory conditions, often yielding reported specific capacitance values exceeding 300–500 F g^{-1} in aqueous electrolytes when evaluated in three-electrode configurations.[16] While such values demonstrate intrinsic charge storage capability, they do not necessarily translate into equivalent performance in practical two-electrode devices. The discrepancy arises from fundamental differences between half-cell and full-cell testing. In symmetric two-electrode systems, the device capacitance is theoretically reduced to one-quarter of the single-electrode capacitance derived from three-electrode measurements, even before accounting for internal resistance and mass balancing constraints.[17] Furthermore, energy density calculations based on single-electrode data often overlook realistic voltage limitations and ohmic losses, leading to inflated projections of device performance. Unlike conventional reviews that predominantly catalogue synthesis strategies and material properties, this review critically examines recent advances in hierarchical pore engineering of waste-derived carbons with a specific focus on understanding and bridging the performance gap between intrinsic material properties and device-level behaviour. We first analyse the fundamental differences between three-electrode and two-electrode evaluation systems, highlighting the origins of performance inflation that arise from low mass loading, restricted voltage windows, electrolyte effects, and the neglect of internal resistance. A quantitative and mechanistic framework is then established to explain the translation of capacitance from single-electrode to full-cell configurations. Building on this, structure–performance relationships are systematically evaluated across multiple studies to identify why materials with ultrahigh surface areas (>2000 m^2 g^{-1}) often fail to deliver superior device performance. Particular attention is given to the roles of pore accessibility, ion transport limitations, electrolyte-pore matching, and the trade-off between porosity and electrical conductivity. The effectiveness of hierarchical pore architectures and heteroatom doping is critically reassessed, distinguishing genuine performance enhancements from overstated effects. Finally, design principles for developing device-relevant carbon electrodes are proposed, emphasising accessible porosity, optimised pore connectivity, and realistic testing conditions. Practical challenges related to scalability, reproducibility, and environmental impact are also discussed. This review provides a comprehensive framework for transitioning from inflated laboratory metrics to reliable, high-performance supercapacitor devices based on waste-derived carbons. Overall, the key contribution of this review lies in establishing a mechanistic and quantitative framework that links intrinsic material characteristics to device-level limitations, including mass-loading effects, ion-transport constraints, electrolyte-pore compatibility, and internal resistance. By integrating insights from multiple studies, this work moves beyond descriptive reporting to identify the underlying factors governing practical performance. Furthermore, this review redefines structure–performance relationships by distinguishing between apparent and effective capacitance, thereby challenging the widely held assumption that higher surface area or hierarchical porosity necessarily translates to superior device performance.

2. Waste-derived carbon materials for supercapacitors

Supercapacitors store energy through either electrical double-layer capacitance or pseudocapacitance mechanisms. The former relies on the electrostatic adsorption of ions at the electrode–electrolyte interface, while the latter involves fast, reversible faradaic reactions occurring at the surface of electrode materials.[8,18] Carbon-based materials, particularly those derived from waste, are favoured for supercapacitor electrodes due to their high surface area, excellent electrical conductivity, and cost-effectiveness.[9,19] Their tunable pore structures and surface chemistries further allow for optimisation of ion transport and electrochemical activity, respectively.[20] The utilization of waste biomass as a precursor offers a compelling avenue for creating sustainable and economically viable electrode materials, often exhibiting unique pore structures and heteroatom incorporation directly from the biomass itself. This approach not only addresses environmental concerns related to waste management but also leverages the intrinsic advantages of waste to produce carbon materials with inherent features beneficial for supercapacitor applications.[21] Specifically, electric double-layer capacitors, which are based on carbon materials, primarily store charge through the rapid adsorption and desorption of electrolyte ions on the electrode surface, offering high power density, excellent cyclic stability, and superior rate performance compared to pseudocapacitors, which rely on faradaic redox reactions.[22]

2.1 Waste-derived carbon precursors for supercapacitors

As highlighted above, utilising waste as a precursor for carbon materials offers a sustainable and economical approach to developing high-performance supercapacitor electrodes. The intrinsic characteristics of waste, such as its lignocellulosic composition in biowaste, facilitate the creation of activated carbons with high surface areas and hierarchical porosities ideal for efficient ion transport and storage in supercapacitor applications.[23] Furthermore, the tailoring of microstructural characteristics of these carbon materials can significantly enhance

various electrochemical properties. Additionally, the inherent heterogeneity and complex structure in various precursors provide a natural template for developing intricate pore networks and diverse surface functionalities, which are highly beneficial for electrochemical performance. These sustainable precursors present a compelling alternative to traditional fossil-based or hazardous electrode materials, addressing concerns regarding cost, toxicity, and environmental impact.[24] For these reasons, various types of waste streams, including biowaste, plastic waste, and industrial waste, among others, have been successfully converted into carbon materials with tailored pore structures for supercapacitors.[9]

2.1.1 Biomass-derived carbons. Biomass-derived porous carbons are attracting significant attention as alternatives to fossil-based feedstocks for supercapacitor applications due to their renewable, abundant, cost-effective, and environmentally friendly characteristics.[25] Moreover, the presence of self-doped heteroatoms, good chemical stability, and naturally occurring hierarchical porosity further contribute to their suitability as ideal supercapacitor electrode materials.[26] This focus on biowaste precursors addresses the limitations of conventional carbon materials, such as graphene, carbon nanotubes, and activated carbon, which often incur high production and regeneration costs. Carbon-based materials can be prepared from different types of biomass, which can be classified into four groups based on composition: woody, herbaceous, aquatic, and animal biomass.[27] The biomass generated during the growth and production of woody plants is the primary source of woody biomass. Wood is the most common example of a woody plant, referring to the roots and stems, which are characterised by thick growth that generates a large amount of xylem, and whose cell walls are generally lignified in solid plants.[28] Wood exhibits a multitude of pipeline structures stacked in parallel along its development direction. These pipeline constructions can serve as microreactors, enabling the formation of electrochemically active sites and thereby facilitating the storage of large volumes of electrolyte ions. On the other hand, pipeline channels facilitate the rapid diffusion of electrolyte ions. Furthermore, wood with excellent electrical insulation and ion permeability can be cut to a specific thickness based on actual requirements and used as a separator between the supercapacitor's positive and negative electrodes. The biomass generated during the development and processing of herbaceous plants is the primary source of herbaceous biomass. Herbaceous plants have few lignified cells and underdeveloped xylem in their stems; they are generally classified into agricultural leftovers and energy crops. Agricultural residues are leftovers from the food, fibre, or agricultural sectors, and those used as animal feed. Energy crops are plants grown for use as fuel, such as sugar cane and sorghum. One common biomass generated during the growth of herbaceous plants is crop straw.[29] Crop straw, which is high in nitrogen, phosphate, potassium, calcium, magnesium, and organic matter, contains more than half of the products of photosynthesis. It is a renewable biomass resource with several uses. The organic nitrogen-rich straw can self-activate during pyrolysis in an inert atmosphere, producing nitrogen-doped straw carbon for porous carbon production. It is worth noting that while the porous carbon serves as a site for double-layer formation, the self-doped heteroatom can introduce pseudocapacitance, thereby enhancing overall electrochemical activity through synergistic effects.[30] For instance, the pyrolysis of algae and lignin, readily available biowaste, has successfully yielded carbon-based electrode materials with enhanced specific capacitance, demonstrating the viability of lignocellulosic biomass as a renewable electrode precursor.[31,32] The term "aquatic biomass" primarily refers to biomass that are found in aquatic environment such as lotus, reed, duckweed, purslane, kelp, and algae. On the other hand, hair, flesh, bones, shells, and animal excrement are the most prevalent sources of animal waste biomass. It worth mentioning that the general inherent structural complexity and chemical composition of diverse biomass feedstocks enable the creation of unique carbon architectures that are difficult to achieve through synthetic routes, offering enhanced performance characteristics for energy storage.[33]

2.1.2 Plastic waste-derived carbons. Beyond biomass, the valorisation of plastic waste into carbonaceous materials presents another compelling avenue for sustainable supercapacitor electrode development, addressing the escalating global challenge of plastic pollution. The pyrolysis of various plastic waste streams, such as polyethylene terephthalate and polyvinyl chloride, yields carbonaceous materials with tuneable porosities and surface chemistries critical for efficient charge accumulation and ion transport in supercapacitors.[9] High-temperature treatment, or carbonisation, is typically required to convert plastic waste into carbon-based materials. This process may involve different atmospheres, catalysts, pressure levels, and heating techniques. Plastic waste has been used to create carbon dots, carbon nanotubes, carbon sheets, carbon spheres, graphene, and irregular porous carbon.[34] It is worth noting that the synthesis technique significantly influences the physicochemical characteristics of these materials and their final electrochemical performance. The activation process and the creation of crosslinked structures are two major processes used to enhance the formation of oxygen-containing functional groups and the homogeneity of plastic waste-derived carbon.[35]

2.1.3 Other waste streams for carbon production. In addition to biomass and plastic waste, other diverse waste streams, such as sewage sludge and industrial by-products, also hold significant potential as precursors for engineered carbon materials in supercapacitor applications.[36] These underutilized resources, often rich in organic matter and heteroatoms, can be strategically processed to yield highly porous carbon structures, expanding the toolkit for sustainable electrode manufacturing.[37] For instance, waste materials derived from sugar and distillery industry waste have demonstrated high surface areas and specific capacitances up to 120 F g^{-1} in aqueous KOH electrolyte, showcasing the potential of such industrial by-products.[38]

2.2 Strategies for hierarchical pores engineering in waste-derived carbon

The strategic engineering of hierarchical pore structures within these waste-derived carbon materials is paramount for

optimising their electrochemical performance in supercapacitors. This involves controlling the intricate balance among micropores, mesopores, and macropores, which collectively facilitate efficient ion diffusion, increase surface-area accessibility, and enhance charge-storage kinetics.[7,39] Specifically, micropores contribute significantly to electrical double-layer capacitance by providing extensive surface area for ion adsorption, while mesopores and macropores serve as essential channels for rapid electrolyte ion transport, mitigating diffusion limitations and enabling high power densities.[40] This multi-scale porosity ensures that a large electrochemical surface area is available for charge accumulation while facilitating rapid ionic flux, thereby optimising both energy and power characteristics of the device.

2.2.1 Template approach strategy. Hierarchical pore engineering can be achieved through various template methods, including hard-template, soft-template, and self-assembly/*in situ* approaches, each offering precise control over pore-size distribution and morphology.[41] This tailored pore architecture, therefore, synergistically contributes to high specific capacitance, excellent rate capability, and prolonged cycle life, addressing the critical demands of advanced supercapacitor applications.[42] Among various template methods, hard templating, a widely employed strategy, utilises a pre-formed inorganic or organic template to precisely dictate the pore architecture of the resulting carbon material. This method involves infiltrating carbon precursors into the template's pores, followed by carbonisation and subsequent removal of the template, thereby creating a negative replica of the template's structure.[4,43] While this approach offers precise control over pore size and morphology, making it valuable for fundamental studies of ion transfer dynamics, its practical applicability is often limited by high costs, time-consuming procedures, and the need for toxic reagents during template removal, thereby hindering large-scale production.[44] Consequently, researchers are increasingly exploring scalable, environmentally benign approaches, such as soft templating and self-templating, to synthesise hierarchical porous carbons with tailored porosity for enhanced electrochemical performance. In contrast to hard templating, soft templating utilises self-assembled organic molecules or polymers as templates, which are typically removed through thermal decomposition, offering a more versatile and often less hazardous route for pore formation.[45] These soft templates, often polymeric or surfactant-based, enable the formation of intricate pore networks by guiding the assembly of the carbon precursor and subsequent pyrolysis. This method enables the generation of hierarchical meso–meso and macro–mesopore structures, which are advantageous for supercapacitor applications owing to their optimised ion-transport pathways and high surface areas.[46,47] This approach allows precise control over pore diameter and distribution, thereby enhancing ionic kinetics and specific capacitance. Furthermore, the removal of soft templates is generally less tedious and less environmentally impactful than that of hard templates, often involving simple thermal treatment without harsh chemical etching, making it a more attractive option for sustainable production.[1,48] Nevertheless, the versatility of soft templating in tailoring pore characteristics through the judicious selection of surfactants and carbon precursors remains challenging. Self-assembly and *in situ* strategies offer an elegant route for engineering advanced carbon architectures without resorting to complex, multi-step templating methods.[49] For instance, the strategic integration of self-assembly techniques enables the bottom-up fabrication of highly ordered porous structures by controlling the aggregation of carbon precursors or their interactions with soft templates. Furthermore, *in situ* strategies, such as the direct carbonisation of biomass materials impregnated with activating agents or dopants, enable the simultaneous formation of porous networks and tailored surface chemistries, thereby enhancing electrochemical efficiency. This integrated approach capitalises on the inherent advantages of biomass-derived carbons, which naturally possess hierarchical porosity and can be easily functionalized with heteroatoms, thereby surpassing the performance of commercial activated carbons.[49,50] Specifically, the extreme porosity of these bio-organic materials often necessitates heteroatom doping to overcome limitations in electrical conductivity, energy density, and capacitive performance.[51] Consequently, incorporating heteroatoms like nitrogen, sulfur, boron, oxygen, or phosphorus into the carbon matrix is an effective strategy to enhance electrical conductivity, wettability, and redox efficiency through electron-donating or withdrawing functional groups. This targeted modification not only elevates the intrinsic electrical properties of the carbon but also introduces pseudocapacitive effects, further enhancing charge storage capacitance through surface redox reactions.

2.2.2 Activation approach strategy. Given the pivotal role of porosity in supercapacitor performance, activation methods are critical for developing hierarchical pore structures with optimised micro-, meso-, and macropore distributions. This multimodal porosity is crucial for enhancing specific capacitance, rate capability, and cycle stability by facilitating rapid ion transport while providing abundant active sites for charge accumulation.[52] Specifically, chemical activation, often employing agents such as KOH, H_3PO_4, or $ZnCl_2$, effectively etches the carbon matrix, creating a high density of micropores and mesopores and significantly increasing the specific surface area available for ion adsorption. Alternatively, physical activation, typically involving steam or CO_2 at elevated temperatures, selectively gasifies amorphous carbon regions, leading to the development of a more ordered graphitic structure alongside controlled porosity. These activation techniques are often combined or optimised to yield hierarchical porous carbon materials that balance high specific surface area with efficient access of electrolyte ions, thereby maximising energy and power densities in supercapacitor applications.[41] Moreover, integrating physical activation methods after chemical treatments can further optimise pore connectivity and introduce larger mesopores and macropores, thereby facilitating electrolyte permeation and reducing ion diffusion pathways within the carbon matrix. The judicious selection and optimisation of activation parameters are therefore paramount for tailoring porous carbon architectures from biowaste, ensuring a balance among enhanced surface area, optimal pore-size distribution,

and improved electrical conductivity to achieve superior electrochemical performance.

2.2.3 Hybrid approaches. Hybrid approaches aim to precisely engineer multi-level porosity by combining different strategies, thereby achieving an optimal balance between micropores for charge storage and mesopores/macropores for rapid ion transport.[53] This can involve dual-template methods utilizing both hard and soft templates to precisely control pore formation across various scales.[54] Additionally, the synergistic combination of chemical activation with physical methods, such as steam or CO_2 activation, can further refine pore size distribution, leading to enhanced ion accessibility and charge transfer kinetics within the electrode material.[20] Moreover, the intentional incorporation of heteroatoms during these hybrid processes can significantly improve the material's intrinsic capacitance and rate capability by introducing additional active sites and modulating the electronic structure of the carbon matrix. Therefore, leveraging advanced synthesis techniques to precisely control the pore architecture and surface chemistry of these materials is paramount for unlocking their full potential in high-performance supercapacitors.

A systematic comparison of synthesis strategies reveals that although numerous approaches have been developed to engineer hierarchical pore structures, their effectiveness varies significantly when evaluated under practical device conditions (Table 1). Hard templating methods offer precise control over pore architecture but are limited by low scalability and the use of hazardous chemicals, making them less suitable for large-scale applications. Soft templating provides improved tunability but often involves complex synthesis procedures and limited reproducibility. In contrast, chemical activation remains the most widely adopted strategy due to its simplicity and ability to generate high surface areas; however, it frequently produces excessive microporosity, which can restrict ion accessibility in thick electrodes and lead to performance overestimation in three-electrode systems. Physical activation methods, while producing comparatively lower surface areas, tend to yield more stable and accessible pore networks that are better suited for practical device configurations. Hybrid approaches that integrate activation, templating, and heteroatom doping show the greatest potential for balancing pore accessibility, conductivity, and scalability. Nevertheless, their practical implementation remains constrained by synthesis complexity and cost considerations. These observations highlight that the choice of synthesis strategy should not be guided solely by maximising surface area, but rather by its ability to deliver accessible porosity and stable performance under realistic operating conditions.

2.3 Principles of energy storage in supercapacitors and performance evaluation

Supercapacitors predominantly store energy *via* two principal mechanisms: electrostatic accumulation of ions at the electrode–electrolyte interface, characteristic of electric double-layer capacitors, or through rapid and reversible faradaic reactions occurring on the electrode surface, defining pseudocapacitors.[17,55,56] While electric double-layer capacitance primarily relies on physical charge separation, providing high power density, pseudocapacitance involves redox reactions that contribute to higher energy density. In the context of electrical double-layer capacitors, which are often the commercially preferred option, effective charge storage is critically dependent on a high surface area to provide ample adsorption sites for electrolyte ions.[57] This dependence necessitates the strategic engineering of pore networks in carbon electrodes to optimise ion accessibility and transport kinetics, particularly because the dynamics of ionic transport in these porous structures are not yet fully understood. Consequently, advanced theoretical and experimental investigations are imperative to elucidate the intricate ion transport mechanisms within complex porous carbon frameworks, particularly concerning how pore tortuosity, connectivity, and surface chemistry influence ion mobility and charge accumulation.[53] The optimised design of hierarchical pore structures, therefore, represents a critical pathway to bridging the performance gap between ideal three-electrode cell evaluations and practical two-electrode supercapacitor devices, thereby enabling enhanced charge-storage kinetics and overall device efficiency. Specifically, optimising the hierarchical pore architecture to balance high specific surface area with facile ion diffusion pathways is crucial for maximising capacitance and rate performance in practical supercapacitor applications. On the other hand, the performance of supercapacitors is evaluated using several key metrics, including specific capacitance, energy density, power density, equivalent series resistance (ESR), cycling stability, and coulombic efficiency.

2.3.1 Specific capacitance. Specific capacitance is typically determined from galvanostatic charge–discharge measurements and reflects the ability of the electrode material to store charge per unit mass, area, or volume.[58] While high capacitance values are often reported in the literature, these are frequently obtained under non-practical conditions, such as low mass loading or in three-electrode configurations, which do not accurately represent real device performance. Specific

Table 1 Comparison of synthesis strategies for hierarchical pore engineering in waste-derived carbons

S/no	Method	Mechanism	Advantages	Limitations	Scalability
1	Hard templating	Template replication	Precise pore control	Detemplating agents are toxic, expensive	Low
2	Soft templating	Self-assembly	Tunable pores	Complex control	Moderate
3	Chemical activation	Etching and pore formation	High surface area, simple	Pore collapse, low conductivity	High
4	Physical activation	Gasification	Better structure	Lower surface area	High
5	Hybrid methods	Combined approaches	Optimized porosity	Complex synthesis	Moderate

capacitance is the most critical parameter for evaluating the performance of supercapacitor electrode materials. Specific capacitance is typically derived from two primary electrochemical techniques, namely galvanostatic charge–discharge (GCD) and cyclic voltammetry (CV).[59] The GCD method is considered the most reliable for practical performance evaluation as it closely mimics real-world device operation.[58] The gravimetric specific capacitance is calculated using eqn (1).

$$\text{Specific capacitance} = \frac{I\Delta t}{m\Delta V} \quad (1)$$

where I is the applied discharge current (A), t is the discharge time (s), m is the mass of the active material on the electrode (g) and ΔV is the potential window (V) during discharge, typically excluding the initial IR drop (internal resistance) for higher accuracy.[60] On the other hand, the CV method provides insight into the charge storage mechanism across a range of scan rates.[61] The specific capacitance is determined by integrating the area under the CV curve using eqn (2).

$$\text{Specific capacitance} = \frac{\int I\,dv}{v \times \Delta V \times m} \quad (2)$$

where I is the current, v is the scan rate, m refers to the mass loading, and V is the potential window. For materials showing significant faradaic behavior, such as transition metal phosphates, the integral method is often preferred over simple peak current analysis to capture the full redox contribution.[62] Depending on the application, capacitance may be expressed in different units: gravimetric capacitance (standard for evaluating the inherent capacitance of the active material, areal capacitance (crucial for evaluating micro-supercapacitors or electrodes with low mass loading. There are various factors that influence the capacitance performance of supercapacitors. For instance, capacitance generally decreases as the current density or scan rate increases because ions have less time to diffuse into the deeper pores or lattice structures of the electrode. It is important to distinguish between specific capacitance (F g^{-1}) and specific capacity (C g^{-1} or mAh g^{-1}), as these terms are often used interchangeably in the literature despite representing fundamentally different electrochemical concepts.[63] Specific capacitance is the appropriate metric for electric double-layer capacitors and is defined based on electrostatic charge storage, whereas specific capacity is typically used for battery-type materials involving faradaic reactions. Although specific capacity can be derived from capacitance using the relationship $Q = C \times \Delta V$, where Q is charge and ΔV is the voltage window, such conversions are strongly dependent on the operating voltage and may lead to misleading comparisons across different systems.[63] Therefore, in this review, performance metrics are consistently reported in terms of specific capacitance (F g^{-1}) to ensure uniformity and avoid ambiguity in evaluating supercapacitor behaviour. It is important to note that the specific capacitance values obtained from CV and GCD measurements often differ, even for the same material. This discrepancy arises from fundamental differences in measurement principles and time scales.[17] In CV, particularly at high scan rates, the rapid potential sweep can limit ion diffusion into smaller or less accessible pores, resulting in lower effective capacitance.[64] In contrast, GCD measurements are typically conducted at lower current densities, allowing sufficient time for electrolyte ions to penetrate deeper into the porous structure, leading to higher utilisation of the active surface area.[65] Additionally, resistive effects influence the two techniques differently. GCD profiles explicitly reflect internal resistance through the initial IR drop, whereas CV curves may partially mask these losses depending on the scan rate and system kinetics. Furthermore, capacitance derived from CV is obtained by integrating the current response over the potential window, which is sensitive to distortions caused by pseudocapacitive reactions or non-ideal behaviour, while GCD-based calculations rely on the slope of the discharge curve, often providing a more stable and practical estimation.[66] Therefore, discrepancies between CV- and GCD-derived capacitance values should be interpreted in the context of scan rate, current density, electrode thickness, and ion transport limitations. For reliable evaluation, it is essential to consider both methods together and assess their consistency under realistic testing conditions.

2.3.2 Energy density. Energy density is a fundamental parameter in the performance evaluation of supercapacitors, representing the total amount of electrical energy a device can store per unit mass (gravimetric) or volume (volumetric). Energy density is defined as one-half the product of capacitance and the square of the operating voltage (eqn (3)). Given that energy density is strongly influenced by the voltage window, electrolyte stability is crucial.

$$\text{Energy density} = \frac{CV^2}{2} \times \frac{1000}{3600} \quad (3)$$

where ED is the energy density (Wh kg^{-1}), C is the specific capacitance, and V is the voltage.

Therefore, doubling the operating voltage results in a four-fold increase in ED, making voltage expansion a more effective strategy for energy enhancement than simply increasing capacitance.[67] Aqueous electrolytes generally provide high ionic conductivity but are restricted to low voltage windows (~1 V), whereas organic and ionic liquid electrolytes enable higher voltages at the expense of conductivity and cost. Over the years, two main strategies, namely asymmetric device configuration and electrolyte engineering, have been employed to maximise the operating window of SC. In an asymmetric device configuration, a pseudocapacitive cathode is paired with a carbon anode, allowing the device to operate over a wider potential window. For example, asymmetric cells utilising nickel phosphate and graphene foam have been shown to operate at windows as wide as 1.6 V, significantly boosting energy compared to symmetric aqueous systems.[67] Electrolyte engineering strategies adopted to extend electrolyte voltage include transitioning from aqueous to organic or ionic liquid systems, increasing salt concentration in aqueous electrolytes, developing advanced solid-state or hybrid electrolytes, and the addition of redox/nanofluid additives, among others.[55,68–71] Each approach involves trade-offs between voltage, conductivity, safety, cost, and long-term stability, and no single solution

currently satisfies all performance requirements simultaneously. For instance, nitrogen-doped multiporous carbons derived from wood waste have demonstrated high energy densities when tested in these high-voltage organic systems.[72] The energy density is rarely evaluated in isolation; it is typically plotted against power density in a Ragone plot. This plot illustrates the "trade-off" inherent in energy storage: as you attempt to discharge the device faster (increasing power), the delivered energy density typically decreases because ions have insufficient time to access all active sites of the electrode materials.[73]

2.3.3 Power density. Power density is also a critical performance metric for supercapacitors, quantifying the rate at which a device can deliver or absorb energy.[74] While batteries excel in energy density, the primary advantage of supercapacitors is their ability to provide high power bursts, which is essential for applications like electric vehicle acceleration and grid stabilization. Power density is typically evaluated in two ways: average power density and maximum power density. The average power density (W kg^{-1}) delivered during a discharge cycle is calculated as the energy density divided by the discharge time (t) (eqn (4)). On the other hand, for assessing the theoretical limits of a material, researchers often calculate the maximum power density, which is governed by the device's internal resistance (eqn (5))

$$\text{Power density} = \frac{\text{energy density}}{t} \times 3600 \quad (4)$$

$$\text{Power density} = \frac{V^2}{4 \times m \times \text{ESR}} \times 3600 \quad (5)$$

where V is the operating voltage, m is the mass of the active material, and ESR is the equivalent series resistance. Some variations in the literature use a factor of 8 in the denominator, depending on the specific cell configuration and ohmic loss considerations.[75]

2.3.4 ESR. ESR is a critical parameter that represents the sum of the intrinsic resistance of the electrode material, the electrolyte resistance, and the contact resistance between the electrode and the current collector. It can be evaluated using electrochemical impedance spectroscopy, where the high-frequency intercept of the Nyquist plot corresponds to the internal resistance. A smaller intercept reflects a lower ESR and more efficient ion transport within the system.[47] GCD profile can also be used to calculate ESR, which is identified by the initial sharp voltage drop (ΔV_{IR}) observed at the start of the discharge curve.[76] It is calculated using eqn (6):

$$\text{ESR} = \frac{\Delta V_{IR}}{2.I} \quad (6)$$

where I is the discharge current. This voltage drop method is highly relevant for practical applications where DC resistance dictates performance.[76] ESR is the primary bottleneck for three key performance metrics: PD, thermal management, and efficiency. While the maximum specific power density of a device is inversely proportional to its ESR, the charging/discharging current through the ESR generates heat that can degrade the electrolyte and electrode materials over time. On the other hand, lower ESR values correspond to higher coulombic efficiency and better charge–discharge reversibility, as less energy is lost to resistive heating.[77] In addition to ESR, the dynamic behaviour of charge transport and storage in supercapacitors can be quantitatively evaluated using the relaxation time constant (τ_0), which is derived from electrochemical impedance spectroscopy. The relaxation time is defined as $\tau_0 = 1/f_0$, where f_0 is the characteristic frequency at which the phase angle reaches $-45°$, marking the transition between resistive and capacitive behaviour.[78–80] Physically, τ_0 reflects the minimum time required for a supercapacitor to discharge all stored energy with an efficiency greater than 50%.[78] A shorter relaxation time indicates faster ion transport within the porous electrode, efficient electrolyte penetration, and minimal diffusion resistance, all of which are critical for high-power performance. Conversely, a larger τ_0 suggests sluggish ion diffusion, poor pore accessibility, and increased resistive losses, particularly in thick electrodes or materials dominated by microporosity. In the context of waste-derived carbon materials, τ_0 provides a more realistic descriptor of electrochemical performance than capacitance alone, as it captures the combined effects of pore structure, electrolyte accessibility, and internal resistance.[79,80] Therefore, incorporating relaxation-time analysis is essential for understanding the limitations of charge transport and bridging the gap between intrinsic material properties and practical device performance.

2.3.5 Cycling stability and coulombic efficiency. Cycling stability is another defining characteristic of supercapacitors, particularly for EDLC systems, which can retain capacitance over hundreds of thousands to millions of cycles. In contrast, pseudocapacitive materials often experience capacitance fading due to structural changes, dissolution, or mechanical degradation, leading to rapid performance loss.[52] The poor inherent stability of pseudocapacitive materials is due to several factors, including structural deformation, surface reconstruction, dissolution of electroactive materials, and delamination of electroactive materials from the current collectors, *etc.*[81,82] On the other hand, a related evaluation metric is coulombic Efficiency, which is the ratio of discharge capacitance to charge capacitance (eqn (7)).

$$\eta = \frac{t_d}{t_c} \times 100\% \quad (7)$$

where t_d and t_c are the discharge and charge capacitance, respectively. Coulombic efficiency provides insight into the reversibility of the charge storage process and the extent of parasitic reactions.

Despite substantial progress in understanding the charge storage mechanism and the evolution of performance of supercapacitors, challenges remain in achieving high energy density without compromising power performance and cycling stability, as well as in translating laboratory-scale materials into commercially viable technologies. Addressing these challenges requires not only advances in material design but also the adoption of standardised testing protocols and rigorous mechanistic understanding.

2.4 Origin of performance gap between three and two-electrode systems

A rigorous understanding of the disparity between three-electrode (3E) and two-electrode (2E) electrochemical measurements is essential for interpreting the reported performance of waste-derived carbon materials in supercapacitors (Fig. 1).[83] Although both configurations are routinely employed to evaluate capacitive behaviour, they probe fundamentally different electrochemical environments and, therefore, generate results that are not directly comparable without appropriate correction or contextualization.[59] In a three-electrode configuration, the working electrode is evaluated independently against a reference electrode with a stable and well-defined potential, while a counter electrode completes the circuit. This arrangement effectively isolates the intrinsic electrochemical response of a single electrode material under conditions that minimise external constraints. The potential of the working electrode is precisely controlled relative to the reference electrode, enabling detailed interrogation of charge storage mechanisms, including electric double-layer formation and surface-confined redox processes.[17] Because the counter electrode is typically oversized and designed to be non-limiting, it does not impose significant kinetic or resistive constraints on the system. As a result, the measured current response predominantly reflects the behaviour of the working electrode itself, rather than that of a complete device. By contrast, a two-electrode configuration constitutes a full-cell system in which both electrodes actively participate in charge storage and collectively determine the device's electrochemical performance. In this setup, there is no independent reference electrode; instead, the applied voltage is shared between the two electrodes, each operating within its own potential window.[17,84] The measured capacitance therefore corresponds to the combined response of the positive and negative electrodes, as well as contributions from internal resistance, electrode–electrolyte interfaces, and mass transport limitations within the entire cell architecture. Consequently, the two-electrode configuration inherently captures device-level behavior, including factors such as electrode balancing, electrolyte stability, and equivalent series resistance (ESR), which are absent or negligible in three-electrode measurements.

These fundamental differences in measurement philosophy give rise to a systematic discrepancy in reported performance metrics. In three-electrode systems, the absence of a second active electrode eliminates the need for charge balance considerations, allowing the working electrode to operate under conditions that maximise its apparent capacitance. The entire potential window is effectively assigned to a single electrode, enabling higher utilisation of surface area and active sites. In contrast, in a two-electrode device, the total voltage must be shared between the two electrodes, and the device's capacitance is governed by the series combination of the individual electrode capacitances. For symmetric systems, this results in a theoretical reduction of the measured capacitance to approximately one-quarter of the value obtained from a single-electrode measurement, even before accounting for resistive losses and inefficiencies. This intrinsic scaling effect is a direct consequence of the electrostatic and electrochemical coupling between the two electrodes in a full-cell configuration.[85]

Beyond these geometric and electrical considerations, several additional factors contribute to the inflation of performance metrics in three-electrode measurements. First, the mass loading of the active material is typically much lower in half-cell studies, often on the order of 1–2 mg cm^{-2} or less, which facilitates rapid ion diffusion and minimizes transport limitations within the porous structure.[86] Under such conditions, even microporous networks that would otherwise suffer

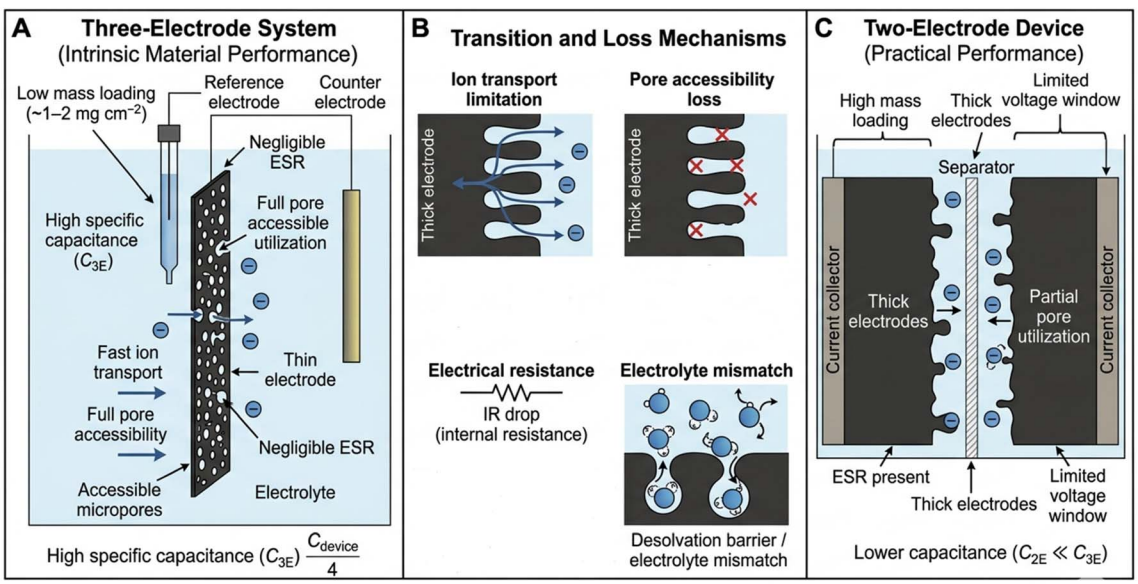

Fig. 1 Schematic representation of the (A) three-electrode configuration, (B) loss due to transition from three-electrode to two-electrode configuration and (C) limitation under two-electrode evaluation of waste-derived porous carbon electrodes.

from restricted ion accessibility in practical devices can exhibit high apparent capacitance. In contrast, real devices require significantly higher mass loadings to achieve meaningful energy density, which introduces diffusion constraints, increases internal resistance, and reduces the effective utilization of the electrode surface. Second, the three-electrode configuration does not adequately capture the impact of electrode thickness and tortuosity on ion transport.[87] In a full device, ions must traverse a complex porous network across both electrodes, and the cumulative diffusion resistance can become a dominant limiting factor, particularly at high current densities.[88] This effect is largely suppressed in half-cell measurements, where the thin working electrode and excess electrolyte volume reduce transport barriers and create conditions that are not representative of practical operation.[89] Third, the influence of internal resistance is significantly underestimated in three-electrode systems. The absence of a realistic electrode pairing and the use of highly conductive current collectors and electrolytes result in minimal ohmic losses.[90] In contrast, two-electrode devices inherently incorporate multiple sources of resistance, including contact resistance between the electrode and current collector, ionic resistance within the electrolyte, and electronic resistance within the porous carbon matrix.[79] These resistive elements manifest as voltage drops during charge–discharge cycling, thereby reducing the effective voltage window and lowering the calculated energy density. Finally, the electrochemical stability window is often overestimated in three-electrode measurements. Because the working electrode potential is controlled independently, it is possible to operate within a narrow, optimised potential range that avoids electrolyte decomposition.[91] However, in a two-electrode device, the total cell voltage is constrained by the stability limits of both electrodes and the electrolyte simultaneously. This often necessitates operating at lower voltages than those implied by half-cell data, further contributing to the discrepancy in energy density between the two configurations.[92] Taken together, these considerations demonstrate that three-electrode measurements inherently provide an idealised representation of electrode performance, emphasising intrinsic material properties while suppressing practical limitations associated with device integration. While such measurements are indispensable for mechanistic studies and material screening, their direct translation to device-level performance is non-trivial and frequently leads to overestimation. A quantitative and mechanistic understanding of these differences is therefore essential for bridging the gap between laboratory-scale evaluation and real-world supercapacitor application.

3. Structure–performance trends in waste-derived carbons for supercapacitors

Pore structures in carbon-based materials are categorised by size into micropores, mesopores and macropores, each contributing distinctly to the electrochemical performance of supercapacitors.[93] Micropores (pore diameter < 2 nm) are critical for charge accumulation due to their high surface area, while mesopores (2 nm < pore diameter < 50 nm) facilitate ion transport, reducing diffusion limitations at high current densities. Macropores, on the other hand, play a crucial role in buffering ions and providing efficient mass transport pathways throughout the electrode architecture, especially in thicker electrodes or high-power applications.[94] This nuanced interplay between pore sizes is essential for optimising both the energy and power density of supercapacitors, enabling them to operate efficiently across a wide range of current densities.[57] Specifically, the contribution of mesopores becomes increasingly significant when the mesopore-to-micropore ratio exceeds a certain threshold, thereby enhancing specific power and energy capabilities. This highlights the importance of a finely tuned balance between these pore classifications to optimise both ion storage and transport kinetics. Therefore, hierarchical pore engineering is a critical strategy in the development of waste-derived carbon electrodes, as it integrates a multi-scale network of micropores, mesopores, and macropores to optimise electrochemical performance.[95] In view of this, numerous researchers have successfully fine-tuned the electrochemical performance of waste-derived carbon by hierarchical pore engineering. For instance, Juan *et al.*,[96] synthesised hierarchical porous carbon from vinegar residue *via* a carbonisation–KOH activation process. The resulting material exhibited a well-developed micro-mesoporous structure, leading to a high specific surface area and enhanced electrochemical performance. This study demonstrates how combined carbonisation and chemical activation can effectively tailor pore architecture for improved ion accessibility and charge storage. The optimised carbon (VRPC 800-2-2) exhibits a high specific surface area of 2133.7 $m^2 g^{-1}$ and a total pore volume of 0.734 $cm^3 g^{-1}$, with a pore size distribution dominated by micropores, accompanied by mesoporous channels. As a result of this hierarchical pore design, the material exhibits a high specific capacitance of 351 F g^{-1} at 0.5 A g^{-1} in a three-electrode configuration, with reasonable rate capability at higher current densities. A symmetric supercapacitor assembled using VRPC 800-2-2 delivered an energy density of 10.5 Wh kg^{-1} at a power density of 275.0 W kg^{-1}, along with excellent cycling stability. Bhat *et al.*[75] converted waste tea leaves into hierarchical porous activated carbon through a two-step activation strategy involving $ZnCl_2$ chemical activation, followed by CO_2 physical activation. During synthesis, $ZnCl_2$ acts as a dual agent, both dehydrating and pore-forming, promoting structural rearrangement of the carbon matrix during pyrolysis, while the subsequent CO_2 activation stage enlarges existing pores and improves pore connectivity. The combined activation approach enables systematic tuning of the pore architecture by varying the $ZnCl_2$/precursor ratio, which directly influences particle morphology, pore size distribution, and surface area development. The morphological analysis reveals that increasing $ZnCl_2$ loading level transforms the carbon structure from compact, low-porosity particles to highly porous spherical carbon frameworks (Fig. 2). The optimised sample (Zn-1) possesses a well-developed hierarchical pore structure with a specific surface area of approximately 1001 $m^2 g^{-1}$. The fabricated

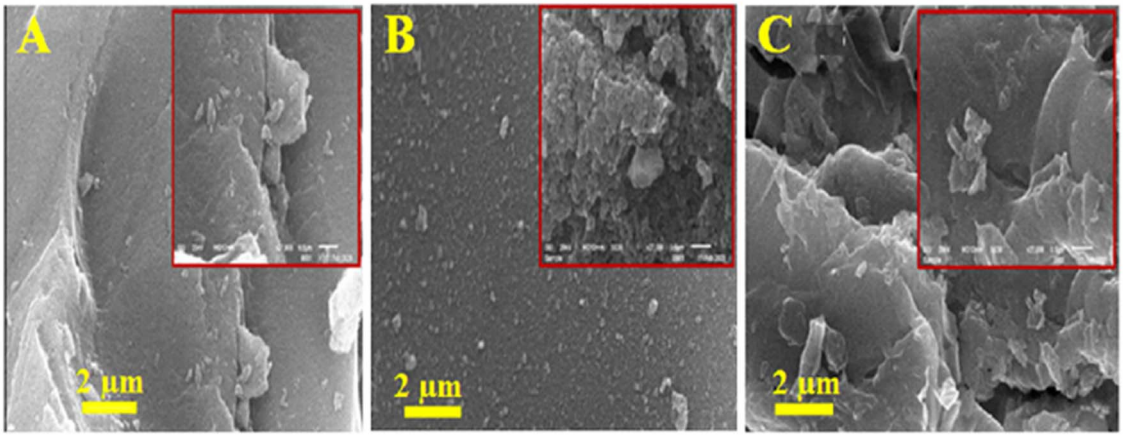

Fig. 2 (A–C) Images of FESEM of activated carbon designed from various weight ratio of tea leaves powder and activating agent $ZnCl_2$; (A) 1 : 0.5 (Zn-0.5), (B) 1 : 1 (Zn-1), (C) (1 : 3 (Zn-3). Reproduced with permission from (ref. 75). Copyright 2025, Elsevier.

symmetrical device with a loading level of 1.15 mg cm^2 delivered a high specific capacitance of 282 F g^{-1} at 0.9 A g^{-1}, an energy density of about 28.3 Wh kg^{-1} at a power density of approximately 35 kW kg^{-1}. Wang prepared a nitrogen-doped porous carbon synthesised from the calyx husk of *Physalis peruviana via* a combined carbonisation–activation–doping process using K_2CO_3 as the activating agent and dicyandiamide as the nitrogen source.[72] During the simultaneous activation and doping stage, dicyandiamide decomposes and incorporates nitrogen into the carbon lattice, while K_2CO_3 promotes pore formation through chemical etching and gas evolution. This synergistic process results in a nitrogen-enriched porous carbon with a hierarchical micro–meso–macroporous structure. The optimised material (NPPCPC-1) exhibits a relatively high nitrogen content of 11.28%, along with a specific surface area of 1677.19 m^2 g^{-1} and a pore volume of 0.85 cm^3 g^{-1}. The NPPCPC-1 electrode delivers a high specific capacitance of 387.9 F g^{-1} at 0.5 A g^{-1} in a three-electrode configuration and maintains over 60% capacitance retention at 50 A g^{-1}, indicating good rate capability. It's worth mentioning that although the specific surface area decreases compared to the undoped sample due to partial pore blocking by dopant species, the enhanced surface chemistry compensates for this loss by introducing additional active sites and improving electrolyte wettability. Therefore, surface-controlled processes dominated the capacitance contribution, suggesting that heteroatom doping enhances fast charge-storage kinetics. In a symmetric configuration, the device exhibits a capacitance of 84.7 F g^{-1} in KOH electrolyte and achieves an energy density of 10.84 Wh kg^{-1}, while maintaining excellent cycling stability, with 99.02% retention after 20 000 cycles. Heteroatom doping has emerged as a key strategy to enhance the electrochemical performance of biomass-derived carbon by modulating surface chemistry and electronic structure. In an attempt to avoid the use of a dopant agent, Taer *et al.*,[97] utilised turnip waste with inherent heteroatoms, including oxygen, phosphorus and sulfur and prepared a multi-heteroatom-doped porous carbon (BACOPS-*x*) *via* a $ZnCl_2$-assisted activation combined with dual-gas (N_2/CO_2) thermal treatment. The resulting carbon exhibits a hierarchical nanofiber-based porous architecture with a moderate specific surface area of 648.7 m^2 g^{-1}, which is lower than that of many KOH-activated carbons but is structurally well balanced. The SEM analysis reveals a three-dimensional, interconnected network composed of short nanofibers and hexagonal pore structures, thereby enhancing electrical conductivity and ion transport. The optimised sample (BACOPS-5) delivers a specific capacitance of 218 F g^{-1} at 1 A g^{-1} in a symmetric configuration and exhibits an energy density of 24.87 Wh kg^{-1} and a power density of 712.65 W kg^{-1}.

Wu and his coworkers demonstrated that $KMnO_4$-assisted activation is an effective approach for generating hierarchical porous carbon with high surface area and enriched oxygen functionality.[98] Indeed, they prepared oxygen-enriched porous carbon from Platanus fibres *via* a two-step carbonisation–activation process using $KMnO_4$ as both an activating agent and surface modifier.[98] During thermal activation, $KMnO_4$ undergoes decomposition to generate MnO_2, MnO, and oxygen species, which chemically etch the carbon framework and produce a well-developed porous structure. This process not only creates abundant micropores but also enlarges some pores into mesopores and macropores through gas evolution and lattice expansion, resulting in a hierarchical pore architecture. The optimised sample (OPF-700-3) exhibits a specific surface area of 1406 m^2 g^{-1}, with a micropore surface area of 1338 m^2 g^{-1} and a total pore volume of 0.64 cm^3 g^{-1}. In a three-electrode configuration, OPF-700-3 delivers a specific capacitance of 318 F g^{-1} at 0.5 A g^{-1}, whereas the device achieves a capacitance of 252 F g^{-1} at 0.1 A g^{-1}, along with an energy density of 7.04 Wh kg^{-1} at a power density of 22.66 W kg^{-1} and excellent cycling stability with 96.5% retention after 20 000 cycles. Although hierarchical pore engineering remains the fundamental strategy for charge storage in biomass-derived carbon materials; however, its effectiveness is often limited by poor intrinsic electrical conductivity. Given above, Stulasti *et al.*,[99] converted tea waste into activated carbon *via* K_2CO_3 activation, followed by integration with graphite as a conductive additive to address

this limitation. The activation process generated a porous carbon structure with a specific surface area of 853.42 $m^2 g^{-1}$, characterised by a combination of micropores and mesopores that support electric double-layer formation and electrolyte diffusion. The SEM analysis confirms the coexistence of porous activated carbon particles and graphitic platelets within the composite, indicating physical mixing rather than chemical bonding. The progressive addition of graphite modifies the microstructure by introducing conductive pathways, as reflected by the significant increase in electrical conductivity. The composite electrodes with moderate graphite content (SC-20) achieve optimal performance, delivering a specific capacitance of 89.62 F g^{-1} at a current density of 0.1 A g^{-1} and an energy density of 17.92 Wh kg^{-1} at a power density of 35.29 W kg^{-1}. This study demonstrates that maximising surface area alone does not guarantee optimal performance; instead, a balance between ion-accessible porosity and electronic conductivity is required. Excessive graphite addition reduces capacitance due to loss of porous surface area, while insufficient graphite limits electron transport. Furthermore, the device is tested in a cylindrical 18 650 full-cell configuration, which inherently includes practical constraints such as electrode thickness, packing density, and internal resistance. Wang *et al.*,[74] reported the conversion of wood waste into nitrogen-doped graphite-like multiporous carbon (N-GMPC) using a one-step activation approach involving KOH and oyster shell powder without inert gas protection. While the high-temperature activation (up to 900 °C) in the presence of KOH induces pore formation through chemical etching, the potassium intercalation promotes the growth of graphitic microcrystals. Simultaneously, nitrogen species originating from protein components in oyster shells are incorporated into the carbon lattice, enabling concurrent pore development, doping, and graphitisation within a single process. A well-developed hierarchical porous structure with abundant micro–mesoporous structures and a specific surface of 1638 $m^2 g^{-1}$ and a pore volume was obtained. In an organic electrolyte (1.0 M SBPBF4/ADN), the symmetric supercapacitor exhibits a specific capacitance of 164 F g^{-1} at a current density of 0.5 A g^{-1} and an energy density of 61.19 Wh kg^{-1} at a power density of 23.22 kW kg^{-1}. A boron-doped nanocarbon (B-NC) was synthesised from coconut husk *via* a two-step process involving high-temperature annealing at 1200 °C followed by hydrothermal boron incorporation using boric acid.[100] The high-temperature treatment promotes partial graphitisation of the carbon framework, while subsequent boron doping introduces electron-deficient sites within the carbon lattice. These p-type defects modify the electronic density distribution and enhance charge carrier mobility, thereby improving conductivity and electrochemical activity. The B-NC electrode delivers a high specific capacitance of 539.5 F g^{-1} at 0.5 A g^{-1}, indicating a substantial pseudocapacitive contribution from boron-induced active sites. The two-electrode device exhibits a specific capacitance of 129.87 F g^{-1} at a current density of 0.5 A g^{-1}, an energy density of 40.5 Wh kg^{-1} at a power density of 7500 W kg^{-1} and good cycling stability for up to 5000 cycles. The excellent electrochemical performance of B-NC is attributed to interconnected nanosheets and densely packed nanostructures that form a porous architecture with overlapping carbon layers as well a specific surface area of 932.6 $m^2 g^{-1}$ with an average pore diameter of ~3.84 nm, suggesting a micropore-dominated structure with mesoporous contributions for ion transport. These studies demonstrates that hierarchical pore engineering alone is insufficient for achieving optimal device performance and must be complemented by graphitization and heteroatom doping. Bamboo waste-derived carbon was synthesised *via* a one-step carbonisation–activation process using K_2CO_3 as a mild activator, with urea and Na_2HPO_4 serving as nitrogen and phosphorus sources, respectively.[101] This integrated approach enables simultaneous pore development and heteroatom incorporation, simplifying the synthesis while ensuring homogeneous dopant distribution. The optimised sample, NP(1 : 1)-HPC, exhibits a hierarchical porous structure with a specific surface area of 1192 $m^2 g^{-1}$ and a pore volume of 0.74 $cm^3 g^{-1}$, combining micropores for charge storage with mesopores for ion transport. The NP(1 : 1)-HPC electrode delivered a specific capacitance of 386.6 F g^{-1} at 0.2 A g^{-1} in a three-electrode configuration, and the device exhibited a specific capacitance of 110 F g^{-1} at 0.2 A g^{-1} along with an energy density of 15.2 Wh kg^{-1} at a power density of 179.9 W kg^{-1}. A molten salt-mediated carbonisation–activation strategy was developed by Xu *et al.*,[102] for the conversion of waste wood-based panels. During carbonisation, $CuCl_2$ melts at ~498 °C, forming a liquid-phase coating around the biomass particles that suppresses the volatilisation of nitrogen-containing species. This mechanism significantly enhances nitrogen retention efficiency and carbon yield. Subsequent $KHCO_3$ activation introduces a hierarchical pore structure while maintaining the nitrogen functionalities preserved during the molten salt stage. The resulting carbon (FB–$CuCl_2$/$KHCO_3$-800-1 : 1) exhibits a specific surface area of 1151 $m^2 g^{-1}$ and a well-developed micro–mesoporous network. Electrochemically, the optimised material delivered a specific capacitance of 220 F g^{-1} at 0.1 A g^{-1} and exhibited excellent rate capability, maintaining 37.28 F g^{-1} at 50 A g^{-1}. The enhanced rate performance is primarily attributed to the high proportion of N-6 species, which facilitates fast and reversible redox reactions, while N-Q species improve electronic conductivity. Singh *et al.*,[10] prepared N, S-codoped porous carbon (NS-WSB-AC) from waste sugarcane bagasse *via* a combined liquid-phase activation, gas-phase doping, and CO_2 activation process. Hydrazine and H_2S were employed as nitrogen and sulfur sources, respectively, enabling simultaneous incorporation of heteroatoms during carbonisation (Fig. 3A). The doping process significantly altered the carbon framework by increasing defect density and expanding the interlayer spacing from 0.38 to 0.42 nm (Fig. 3B), facilitating ion intercalation within the carbon matrix. In addition, activation produced a hierarchical micro–mesoporous structure with a high specific surface area of 2455.6 $m^2 g^{-1}$ and a total pore volume of 0.4784 $cm^3 g^{-1}$, in which mesopores enhance ion transport and micropores provide charge storage sites. In a three-electrode configuration, NS-WSB-AC delivers a high specific capacitance of 405.67 F g^{-1} at 0.2 A g^{-1} (Fig. 3C), whereas the asymmetric device delivered a specific capacitance of 220.6 at a current density of 0.2 A g^{-1} and an energy density of

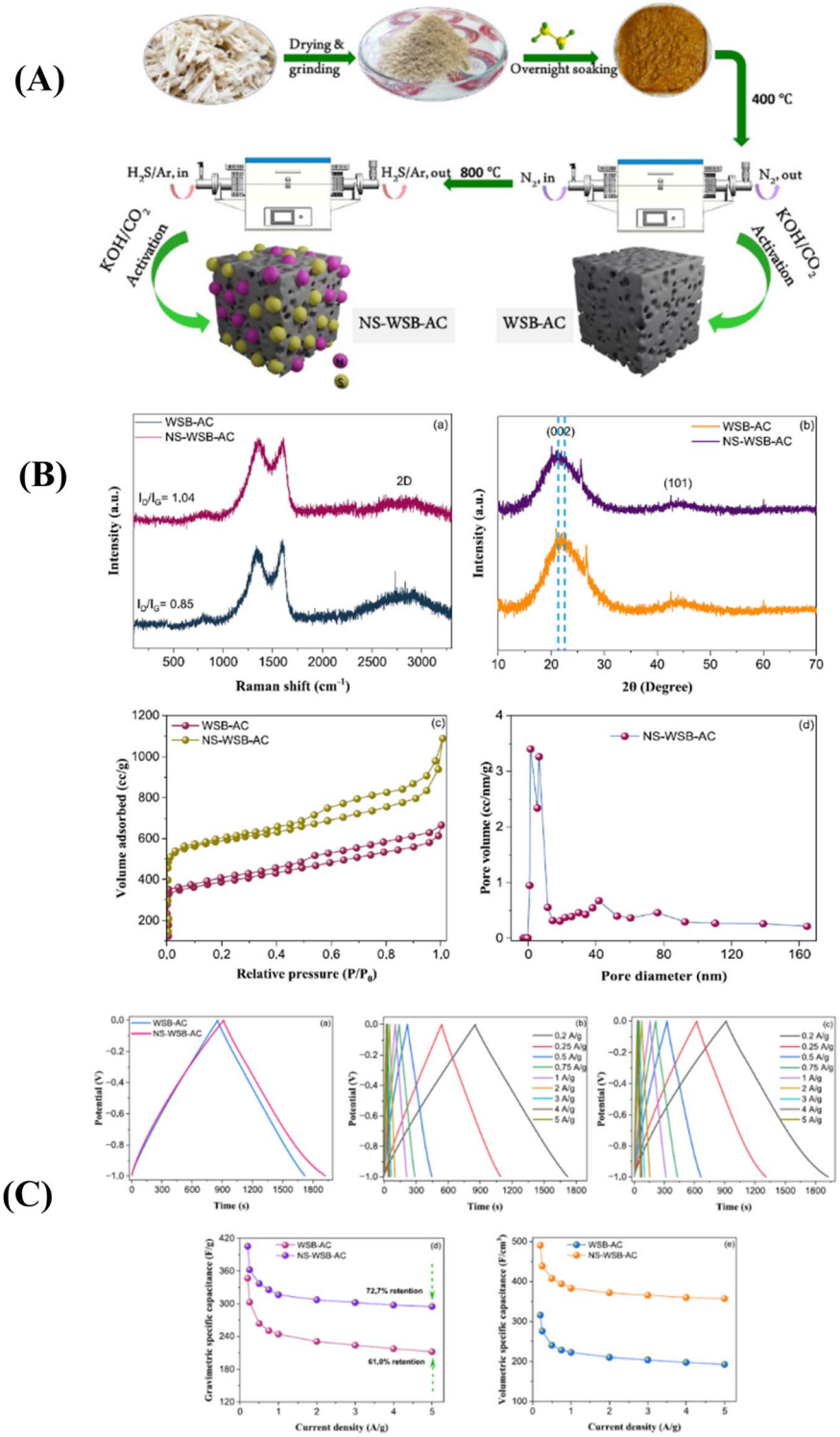

Fig. 3 (A) Synthesis of biomass-derived activated carbon and the processing steps involved in the fabrication of NS-WSB-AC sample. (B) (a) Raman spectra, (b) XRD patterns, and (c) nitrogen adsorption and desorption isotherms of WSB-AC and NS-WSB-AC and (d) BJH pore size distribution curve of NS-WSB-AC. (C) (a) GCD curves of WSB-AC and NS-WSB-AC electrodes in 6 M KOH at 0.2 A g^{-1}, (b) GCD curves of WSB-AC electrode at various current densities, (c) GCD curves of NS-WSB-AC electrode at different current densities, (d) variation of gravimetric specific capacitance, and (e) volumetric specific capacitance as a function of current density for WSB-AC and NS-WSB-AC. Reproduced with permission from (ref. 10). Copyright 2025, Elsevier.

54.73 Wh kg^{-1} at a power density of 207.8 W kg^{-1}. The development of hierarchical porous carbon from biomass precursors remains a key strategy for achieving high electrochemical performance, particularly when combined with intrinsic heteroatom self-doping. A five-eyed kernel was converted into N/O self-doped porous carbon (FKC-800) *via* a one-step pre-

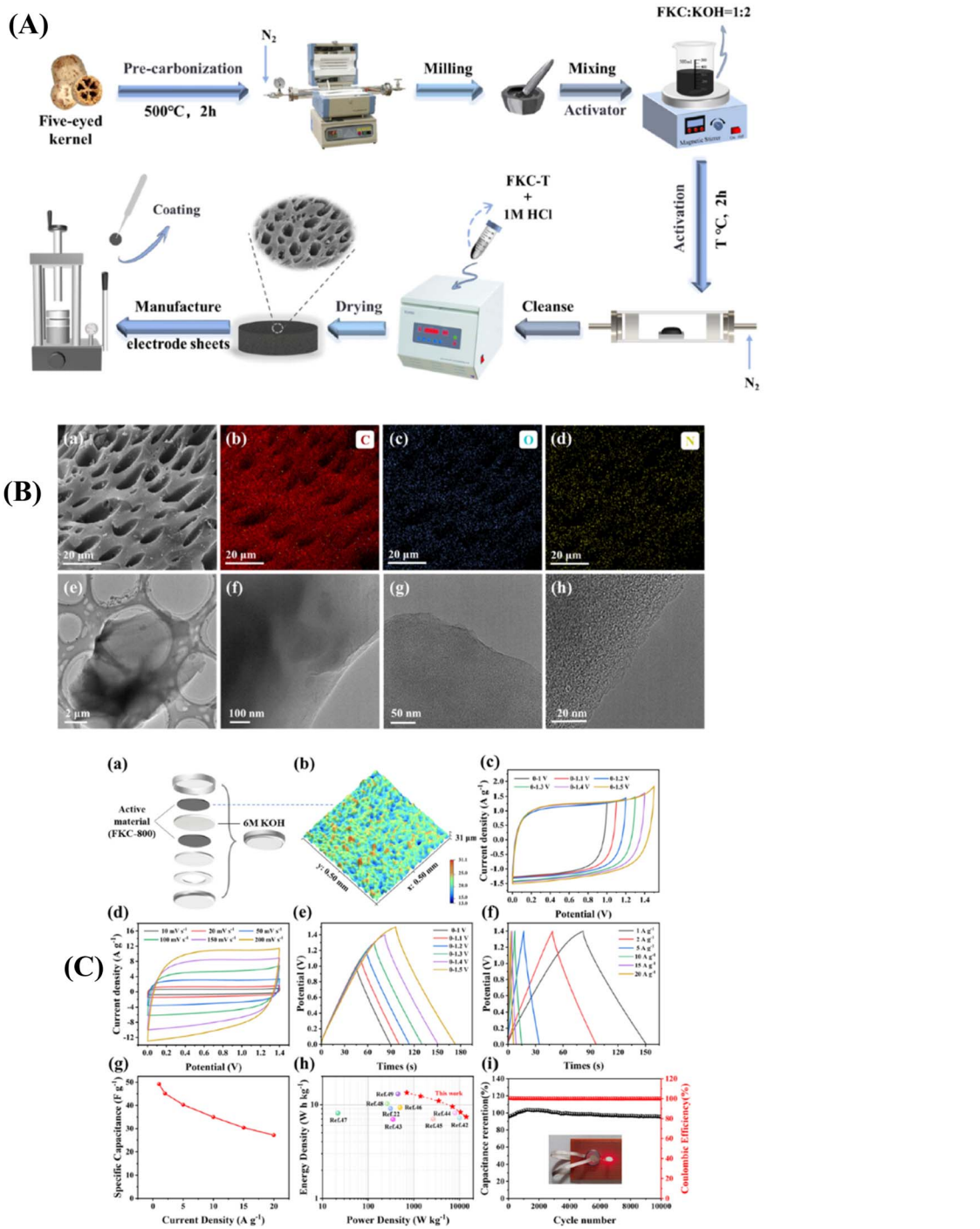

Fig. 4 (A) Preparation of biomass porous carbon from waste five-eyed kernel. (B): (a) SEM images of FKC-800, (b–d) EDS mapping images of FKC-800, (e and f) TEM images of FKC-800, (g and h) HRTEM images of FKC-800. (C) (a) Schematic diagram of button-type symmetric supercapacitor assembly, (b) 3D topography of the electrode surface, (c) CV curves of the devices in different voltage windows at 20 mV s^{-1}, (d) CV curves at different scan rates, (e) GCD curves of the devices in different voltage windows at 1 A g^{-1}, (f) GCD curves at different current densities, (g) specific capacitance of the devices at 1–20 A g^{-1}, (h) Ragone plot and (i) cycling stability of FKC-800 SSC at 1 A g^{-1}. Reproduced with permission from (ref. 36). Copyright 2025, Elsevier.

carbonisation–KOH activation process, in which the activation temperature was systematically tuned to regulate pore structure (Fig. 4A).[36] The SEM and TEM images reveal a highly developed porous structure with interconnected macro–micro channels (Fig. 4B). The optimised sample (FKC-800) achieves a high specific surface area of 1475.36 m^2 g^{-1}, indicating effective pore development, and in a three-electrode configuration, FKC-800 delivers a high specific capacitance of 414.38 F g^{-1} at 1 A g^{-1}. In a symmetric configuration, a device achieves a capacitance of 49.2 F g^{-1} at a current density of 1 A g^{-1}, with an energy density

of 13.4 Wh kg^{-1} at a power density of 700 W kg^{-1}, and excellent cycling stability (95.4% retention after 10 000 cycles) (Fig. 4C).

A porous carbon was synthesised from cow urine *via* a template-free pyrolysis approach, followed by KOH pre-activation to enhance porosity and conductivity.[26] The synthesis involves drying cow urine to obtain a solid precursor, which is subsequently carbonised at 700 °C (CCUR-700) and further activated using KOH to produce a highly porous carbon network (A-CCUR-700) with a high specific surface area of 2651.7 m^2 g^{-1} and a pore volume of 1.47 cm^3 g^{-1}. The symmetric supercapacitor assembled using A-CCUR-700 delivers a capacitance of 165 F g^{-1} at 0.5 A g^{-1}, achieves an energy density of 22.9 Wh kg^{-1} at a power density of 5100 W kg^{-1}, and maintains 95.3% capacitance retention over 5000 cycles, indicating excellent stability. Yue *et al.*,[42] utilised spiral algae as a heteroatom-rich precursor and industrial waste (calcium carbide slag, CCS) as a Ca-based hard template in a one-step carbonisation process assisted by $KHCO_3$ activation to produce multi-heteroatom self-doped carbon (KHSA/CCS). During pyrolysis, $KHCO_3$ decomposes to generate K_2O and CO_2, which chemically etch the carbon framework, while the CCS template plays multiple roles, including *in situ* CO_2 adsorption, structural support, and secondary pore generation. After the acid removal of CCS leaves, a well-developed hierarchical pore structure with micropores, mesopores, and macropores and a high specific surface area of 1911.87 m^2 g^{-1} and a large pore volume of 1.05 cm^3 g^{-1} is obtained (KHSA/CCS-0.2). Notably, heteroatom content is influenced more strongly by pyrolysis temperature than by template addition, indicating that pore regulation and doping are partially decoupled processes. The optimised sample delivers a high capacitance of 344.65 F g^{-1} at 0.5 A g^{-1}, whereas the symmetric supercapacitor exhibits a capacitance of 268.35 F g^{-1} at 0.25 A g^{-1}, along with an energy density of 14.16 Wh kg^{-1} at a power density of 75 W kg^{-1}, and excellent cycling stability (99.05% retention after 10 000 cycles).

The activation process plays a decisive role in structural evolution by removing inorganic impurities and generating porosity through chemical etching and gas evolution, thereby transitioning from a dense, non-porous structure to a highly porous carbon framework. Given the above, Dhanavel *et al.*,[103] converted coconut bracts into activated carbon (ACB) through a two-step carbonisation–KOH activation process, where carbonisation at 550 °C was followed by activation at 700 °C under N_2 atmosphere. The structural characterisation confirms the formation of a hierarchical porous network with interconnected pore channels, with a specific surface area of 767.3 m^2 g^{-1} for ACB, and a pore volume of 0.37 cm^3 g^{-1}. The activated carbon-based electrode delivers a high capacitance of 338 F g^{-1} at 2 A g^{-1} in a three-electrode configuration. In a symmetric configuration, the device achieves a capacitance of 105 F g^{-1} at 1 A g^{-1}, along with a high energy density of 28.58 Wh kg^{-1} at a power density of 6997.72 W kg^{-1}. A porous carbon was synthesised from broad bean husk *via* a two-step process involving CH_3COOH-assisted hydrothermal pretreatment followed by K_2CO_3 activation.[104] The hydrothermal treatment selectively decomposes hemicellulose and lignin, generating initial mesoporous frameworks, while subsequent K_2CO_3 activation promotes extensive pore development through chemical etching. The optimised sample (BBHPC-2) achieves a high specific surface area of 2078.4 m^2 g^{-1} and a total pore volume of 1.17 cm^3 g^{-1}. In a three-electrode configuration, BBHPC-2 delivers a high capacitance of 386.5 F g^{-1} at 0.5 A g^{-1}, whereas the symmetric device achieves a specific capacitance of 283.3 F g^{-1} at 0.5 A g^1, corresponding to an energy density of 28.4 Wh kg^{-1} at a power density of 275 W kg^{-1}. It is worth noting that excessive activation leads to pore collapse, highlighting the importance of controlled activation. Hu *et al.*,[105] adopted a molecular-level strategy to regulate pore evolution by controlling the cleavage of glycosidic bonds in biomass sawdust through an acetic acid/H_3PO_4 synergistic activation system. Acetic acid facilitates the depolymerisation of cellulose and hemicellulose into glycosylated small molecules, significantly reducing the bond dissociation energy. These smaller molecular fragments enhance the accessibility of H_3PO_4, promoting the formation of phospho-biopolymer crosslinked structures during pyrolysis. Upon subsequent carbonisation and washing, these crosslinked intermediates decompose, generating a well-developed hierarchical porous structure with a high specific surface area of 2072 m^2 g^{-1}, a total pore volume of 1.65 cm^3 g^{-1}, and a mesopore volume of 1.04 cm^3 g^{-1}. The optimised electrode (ACPA-3) delivers a specific capacitance of 284 F g^{-1} at 0.5 A g^{-1} in a three-electrode system. The device achieves an energy density of 6.89 Wh kg^{-1} at a power density of 290.78 W kg^{-1}, with good cycling stability (~84% retention after 10 000 cycles). The performance enhancement is attributed to the synergistic effect of micropores for charge storage and mesopores for ion diffusion, as well as improved pore connectivity resulting from molecular-level precursor regulation. It is worth noting that the introduction of acetic acid significantly increases mesoporous volume compared with conventional H_3PO_4 activation. In addition to the activation agent, chemical exfoliation, combined with hierarchical pore engineering, significantly enhances the structural accessibility and electrochemical performance of waste-derived carbon. Tea saponin extracted from camellia oleifera residue was converted into N, O-doped porous carbon *via* a urea-assisted $KHCO_3$ activation strategy.[106] During thermal treatment, $KHCO_3$ decomposes, releasing CO_2 and H_2O and generating internal pressure that promotes pore formation and interlayer expansion, while potassium intercalation weakens van der Waals forces between carbon layers (Fig. 5A). Simultaneously, urea decomposition produces NH_3 and intermediate species that delay $KHCO_3$ decomposition and introduce additional gas-stripping effects, thereby further enhancing exfoliation.[106] This synergistic mechanism transforms the precursor from bulk carbon into thin, layered porous carbon sheets with a highly accessible hierarchical pore structure (Fig. 5B), a specific surface area of 1727 m^2 g^{-1}, and a large pore volume of 1.334 cm^3 g^{-1}, with micropores accounting for 55.2% of the total pore volume. When employed as electrode material, it delivers a high specific capacitance of 388 F g^{-1} at 0.5 A g^{-1}, with good rate capability. A symmetric device exhibits a capacitance of 187 F g^{-1} at 0.5 A g^{-1}, with an energy density of 43.9 Wh kg^{-1} at a power

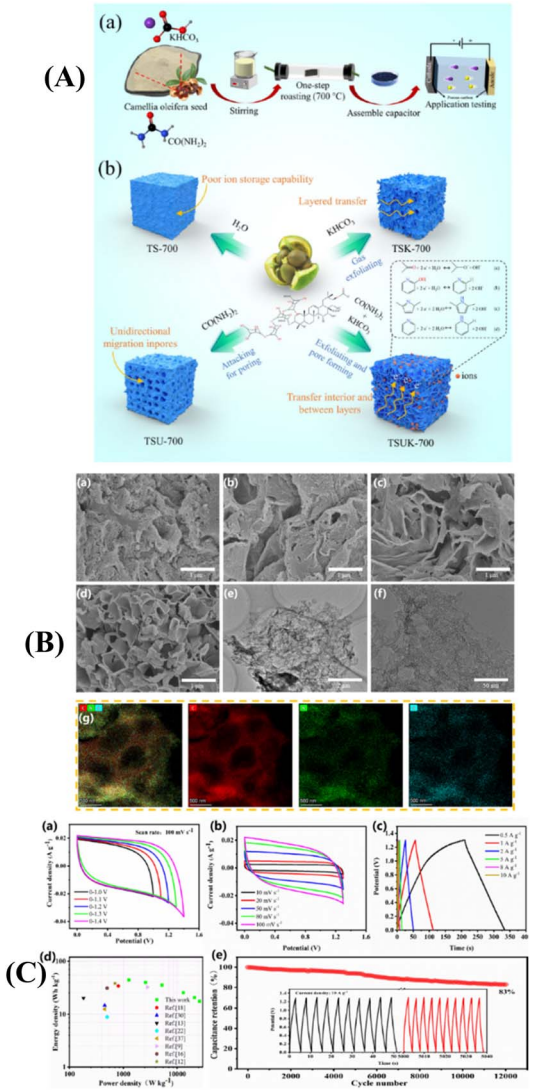

Fig. 5 (A) (a) Schematic illustration for the synthesis of tea saponin (TS)-derived carbon materials. (b) Formation and electrochemical storage mechanism of TS-derived porous carbon. (B) Structure characterisation of TS-derived carbon. SEM images of (a) TS-700, (b) TS urea (TSU-700), (c) TS potassium (TSK-700) and (d) TSUK-700. TEM images of (e) and (f) TSUK-700. (g) The C, O, N element mapping of TSUK-700. (C) Electrochemical measurements of the TSUK-700 electrode with a two-electrode system in 6 M KOH electrolyte. (a) Detection of voltage window, (b) CV curves, (c) GCD curves, (d) Ragone plot calculated in the current density range of 0.5–10 A g^{-1} in comparison with the reported results and (e) the cycling stability, determined from GCD tests at 10. A g^{-1} (the insets show the first ten cycles and the last ten cycles, respectively). Reproduced with permission from (ref. 106). Copyright 2025, Elsevier.

density of 1275 W kg^{-1} and excellent cycling stability (Fig. 5C). Heteroatom co-doping carbon (NP-AC) was prepared by using corn bracts *via* activation with $NH_4H_2PO_4$, which serves both as a phosphorus source and an activating agent.[107] During pyrolysis, $NH_4H_2PO_4$ decomposes to generate gaseous species and reactive intermediates that promote pore formation, while simultaneously incorporating nitrogen and phosphorus into the carbon lattice. Compared with single-atom doping (N-AC or P-AC) and undoped carbon (AC), co-doping significantly enhances both the pore structure and surface chemistry, indicating a strong synergistic effect between heteroatoms and activation. Among all the samples, NP-AC has the highest specific surface area of 286.5 m^2 g^{-1} and a pore volume of 0.14 cm^3 g^{-1}, thereby delivering a capacitance of 160.1 F g^{-1} at 1 A g^{-1}. A symmetric device exhibits a specific capacitance of 41.4 F g^{-1} at a current density of 1 A g^{-1} and delivers an energy density of 10.5 Wh kg^{-1} at 350 W kg^{-1}.

Bird feathers with varying melanin content were employed as precursors to synthesise activated carbon *via* KOH activation at optimised temperatures, as reported by Verma *et al.*[108] In this study, the key design concept is melanin-driven heteroatom incorporation, in which nitrogen- and oxygen-containing functional groups inherent to β-keratin and melanin are retained during carbonisation and directly contribute to electrochemical activity. As expected, all samples exhibit hierarchical micro–mesoporous structures, with surface areas ranging from 763 to 1212 m^2 g^{-1}, with the sample obtained from the crow (CF7A7) showing the highest. A key structure–property insight from this study is that capacitance does not scale directly with surface area, but rather depends strongly on heteroatom composition and pore accessibility. Indeed, symmetrical device fabricated using peacock based sample (PF7A7), despite having the lowest surface area (763 m^2 g^{-1}), delivers the highest capacitance ~384 F g^{-1} at current density of 1 A g^{-1} due to its relatively higher nitrogen content (~6%), whereas CF7A7, with the highest surface area (~1212 m^2 g^{-1}), exhibits lower capacitance (~361 F g^{-1}). Furthermore, the device delivers an energy density of 13 Wh kg^{-1} at a power density of 250 W kg^{-1}, with superior rate capability due to lower diffusion resistance. *Setaria viridis* stalks were employed as a precursor, leveraging their natural hollow tubular vascular bundle structure to generate interconnected porous carbon frameworks through carbonisation and KOH activation.[109] It was demonstrated that high-temperature carbonation did not significantly alter the hollow tubular vascular bundle structure, and subsequent activation transformed this structure into a porous honeycomb-like network. Although increasing temperature enhances pore development, excessive activation (1000 °C) leads to structural collapse and pore blockage. The optimised sample (SVS-900) exhibits a micropore-dominated structure with a high specific surface area of 1555.36 m^2 g^{-1} and pore sizes mainly below 1 nm, which are favourable. In a symmetric two-electrode configuration, SVS-900 delivers a capacitance of 230 F g^{-1} at 0.2 A g^{-1} in aqueous electrolyte, while in a flexible solid-state configuration, it achieves 487 F g^{-1} at 2 A g^{-1} and exhibits an energy density of 8.28 F g^{-1} at a power density of 3500 W kg^{-1}. Kish graphite (KG) recovered from blast furnace dust was purified and subsequently converted into graphene-based porous carbon through oxidation, reduction, and KOH activation.[110] The purification process effectively increased the carbon content from ~61% to >95% by removing metallic and non-metallic impurities through magnetic separation, decantation, and acid leaching, yielding a highly crystalline graphite precursor with an interlayer spacing of ~0.34 nm, comparable to that of natural graphite. This highly ordered structure serves as a foundation

for further pore engineering and graphene formation. Structural evolution during activation is primarily governed by KOH-induced chemical etching and lattice expansion. Firstly, KOH activation generates micropores through redox reactions, gas evolution (CO_2/CO), and potassium intercalation, thereby expanding the carbon lattice and producing a porous framework after washing. Nitrogen sorption analysis shows that the surface area increases significantly, indicating successful formation of slit-like micro–mesopore. A device fabricated using the optimised sample (C-rGO) electrode exhibits a specific capacitance of 85.3 at 0.1 mA g^{-1} and an energy density of 7.7 Wh kg^{-1} at a power density of 97 W kg^{-1}. The coexistence of graphitic domains and defect-rich regions in C-rGO could have enabled improved electrical conductivity while maintaining sufficient active sites for charge storage. Although the combination of moderate surface area, hierarchical porosity, and improved conductivity enables efficient charge storage, the capacitance remains limited compared to that of highly activated biomass carbons due to a lower overall surface area. Rice husk was employed as a cellulose-rich precursor to fabricate carbon aerogels (CAs) through a gelation-freeze-drying-carbonisation route, following a two-step pretreatment to remove lignin, hemicellulose, and silica as reported by Atanasio and coworkers.[111] The sol–gel process enables the formation of an interconnected cellulose network, which is preserved during freeze-drying and subsequently converted into a carbon framework upon pyrolysis at 800 °C. This approach differs from conventional activation methods by relying on structural templating from the gel network rather than aggressive chemical etching, resulting in a low-density, three-dimensional porous architecture. Among the synthesised samples, 1B with surface area of 341.73 m^2 g^{-1}, exhibits the best performance, delivering a capacitance of 58 F g^{-1} at 0.1 A g^{-1}, while maintaining good rate capability and cycling stability, as compared to 2 A, which exhibits a higher surface area (728.30 m^2 g^{-1}). This highlights that pore size distribution and connectivity, rather than surface area alone, govern electrochemical performance; thus, a balanced micro–mesoporous structure enables better ion accessibility and more efficient charge storage. In contrast to the above, pineapple stem starch (PSS), an amylose-rich agricultural waste, was employed as a precursor to synthesise activated carbon (SAC-800) *via* a gelatinisation–retrogradation–carbonisation–KOH activation sequence.[58] The gelatinisation process disrupts hydrogen bonding in starch, enabling molecular rearrangement, while ethanol treatment and freezing induce structural stabilisation. Subsequent carbonisation and KOH activation generate a porous carbon framework *via* chemical etching and gas evolution, yielding a worm-like, interconnected porous structure with an ultrahigh specific surface area of 2796 m^2 g^{-1}. In a three-electrode configuration, SAC-800 delivers a specific capacitance of 374 F g^{-1} at 0.1 A g^{-1} and retains 86 F g^{-1} at 5 A g^{-1}, indicating good rate capability despite its micropore-dominated structure. A symmetric coin-cell-based device exhibits a capacitance of only 37 F g^{-1} at 0.1 A g^{-1}, corresponding to an energy density of 5 Wh kg^{-1} at a power density of 49 W kg^{-1}. Pyrolysed carbon black (CBp) is characterised by a high ash content and a low surface area. To unveil its potential application in a supercapacitor, it was converted into activated carbon (ACBp1) *via* acid purification followed by *in situ* SiO_2 template–assisted KOH activation, as reported by Yin *et al.*[112] The purification step selectively removes inorganic impurities (*e.g.*, $CaCO_3$, ZnS), while retaining SiO_2 as an intrinsic hard template. During subsequent activation, SiO_2 reacts with KOH to form K_2SiO_3, which expands within the carbon matrix and acts as a pore-forming agent. After removal, this process generates a hierarchical pore structure with interconnected micro- and mesopores (Fig. 6A). As shown in Fig. 6B, ACBp1 exhibits uniformly dispersed carbon particles with reduced agglomeration, thereby facilitating improved electrolyte accessibility. Furthermore, nitrogen adsorption–desorption analysis of ACBp1 indicates a surface area of 622.9 m^2 g^{-1}, with well-developed hierarchical porosity consisting of micropores and mesopores, thereby delivering a capacitance of 246 F g^{-1} at 1 A g^{-1} (6C). The symmetric supercapacitor achieves a capacitance of 100 F g^{-1} at 1 A g^{-1}, an energy density of 28.4 Wh kg^{-1} at a power density of 710 W kg^{-1}, with good rate capability (62% retention from 1 to 20 A g^{-1}) and excellent cycling stability (~82% retention after 20 000 cycles).

Wang *et al.* adopted a strategy to effectively facilitate the rearrangement of the pore structure and introduce a synergistic combination of non-metallic dopants.[52] In this study, sulfur- and phosphorus-*co*-doped porous carbon (KPC-SP) was synthesised from kiwi fruit peel *via* a one-step KOH activation, combined with thiourea and sodium hypophosphite as dual dopant–activators. During high-temperature activation, KOH induces carbon etching and lattice expansion, generating abundant micropores, while the decomposition of dopants produces gaseous species (NH_3, H_2S, PH_3) that further promote pore formation and structural rearrangement. This dual-function mechanism enables simultaneous pore development and heteroatom incorporation, resulting in a defect-rich carbon framework with optimised surface chemistry. Structural characterisation demonstrates that the optimised sample (KPC-SP-1) exhibits a high specific surface area of 2691.85 m^2 g^{-1} and a large pore volume (~1.27 cm^3 g^{-1}), with a dominant micropore fraction (~78.6%) and additional mesopore contributions. The KPC-SP-1 electrode delivers a capacitance of 323.5 F g^{-1} at 1 A g^{-1}, with good rate capability (86.24% retention at 10 A g^{-1}), indicating efficient ion transport within the hierarchical structure. The symmetric supercapacitor operates over a wide voltage window of 2.0 V and delivers a capacitance of 118.5 F g^{-1} at 1 A g^{-1}, with an energy density of 31.8 Wh kg^{-1} at a power density of 697 W kg^{-1}, and exhibits excellent cycling stability. The activation process could act as both a dehydrating and pore-forming mechanism, promoting the removal of volatile species and facilitating the development of micro-mesoporous structures. In this regard, activated carbon (MKAC) was synthesised from *Murraya koenigii* seeds *via* $ZnCl_2$-assisted chemical activation followed by high-temperature carbonisation (900 °C).[77] $ZnCl_2$ activation transforms dense biomass into porous carbon while preserving structural integrity, resulting in the specific surface area increasing from 432 m^2 g^{-1} (MK) to 798 m^2 g^{-1} (MKAC), while micropore surface area increases from 56 to 428 m^2 g^{-1}, indicating substantial micropore formation. These

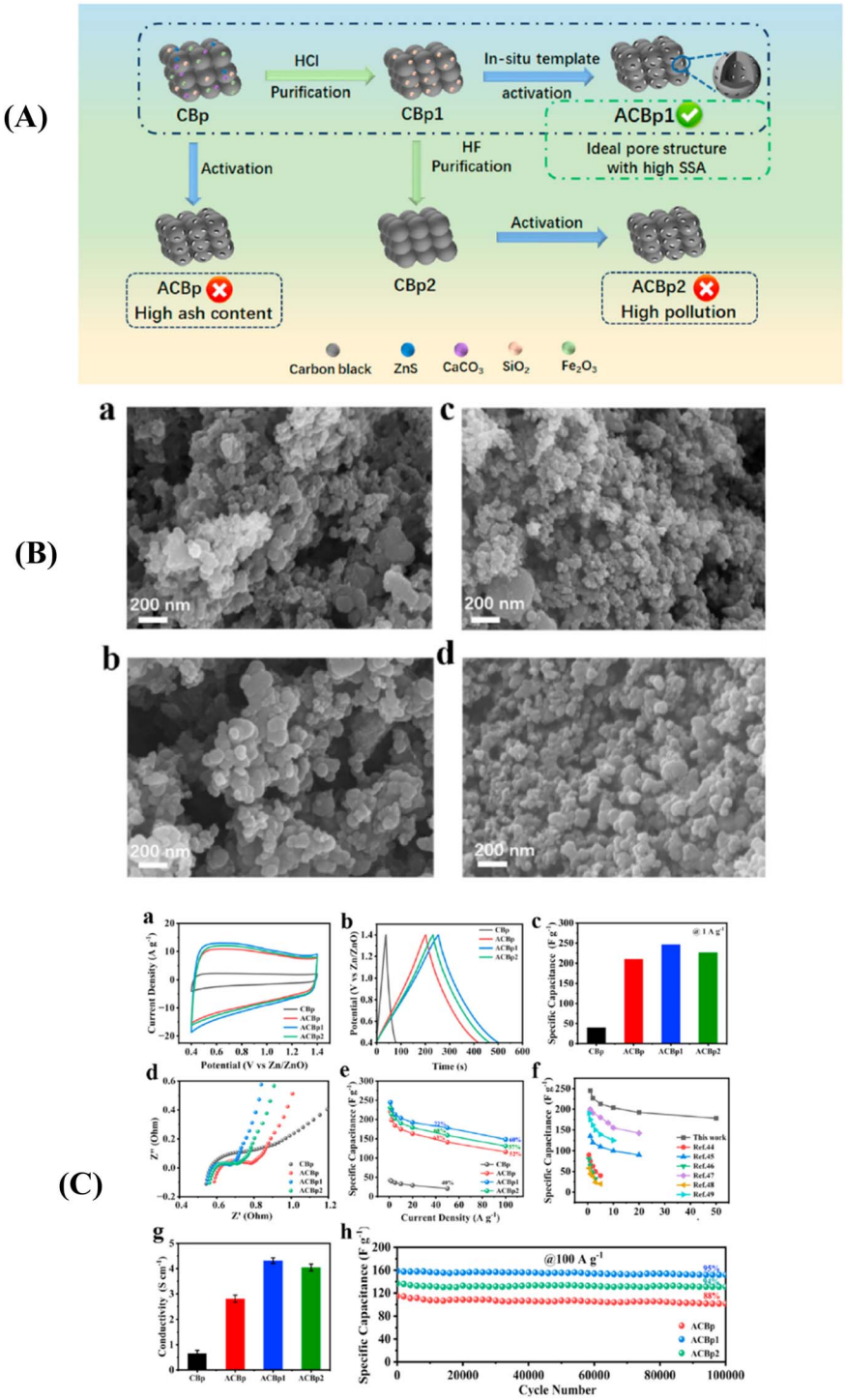

Fig. 6 (A) Schematic diagram of preparation of CBp products. (B) SEM images of (a) CBp, (b) ACBp, (c) ACBp1, (d) ACBp2. (C) (a) CV curves at 50 mV s^{1}, (b) GCD curves at 1 A g^{-1}, (c) specific capacitance at 1 A g^{-1}, (d) Nyquist plots, (e) rate performance, (f) comparison of rate performance with other materials (g) conductivity test, (h) cycle performance at 100 A g^{-1}. Reproduced with permission from (ref. 112). Copyright 2025, Elsevier.

structural features directly influence electrochemical performance, and thus, the MKAC electrode exhibits a specific capacitance of 178.98 F g^{-1} at 0.5 mA cm^{-2} in a symmetric EDLC configuration. Additionally, the device delivers a specific energy of roughly 16.32 Wh kg^{-1} and a power density of around 436 W kg^{-1}. Karademir and Inal reported the preparation of activated carbon (AC) derived from industrial red pepper waste *via* K_2CO_3 activation at 800 °C, followed by integration onto carbon fibre fabrics (CFFs) to develop structural supercapacitor electrodes.[21] The AC exhibits a micropore-dominated

hierarchical structure and a high surface area of 1120.96 $m^2 g^{-1}$. Unlike conventional particulate electrodes, the AC is applied as a coating onto carbon fibre fabrics, forming a hybrid hierarchical architecture. This configuration integrates two structural functions: the carbon fibres provide mechanical integrity and conductive pathways, while the activated carbon layer supplies high surface area and porosity for charge storage. As a result, electrochemical performance is governed not only by pore structure but also by the distribution and accessibility of the AC coating. The capacitance increases significantly with AC loading, reaching 4.59 F g^{-1} at 0.015 A g^{-1} for 10% AC–CFF, compared to 0.24 F g^{-1} for unmodified CFF and an energy density of 0.102 Wh kg^{-1} at a power density of 3000 W kg^{-1}. A 3D honeycomb-like porous carbon (CSPC-*X*) was prepared using waste chrysanthemum stems.[113] Among the samples, CSPC-2 exhibited the most uniform and interconnected architecture, exhibiting a well-developed hierarchical pore structure with a high specific surface area of 1710.8 $m^2 g^{-1}$ and a total pore volume of 1.14 $cm^3 g^{-1}$, where mesopores account for ~71.1% of total pore volume. In a three-electrode configuration, CSPC-2 delivers a high capacitance of 366.5 F g^{-1} at 0.5 A g^{-1}, whereas the symmetric device achieves a capacitance of 272.9 F g^{-1} at 0.5 A g^{-1}, along with an energy density of 18.7 Wh kg^{-1} at a power density of 325 W kg^{-1}. In addition to biomass, polymeric waste can be transformed into functional carbon materials with enhanced electrochemical performance. For instance, waste polypropylene medical masks were converted into sulfur-doped porous carbon *via* a sulfonation–ball milling–KOH activation–carbonisation process.[3] The sulfonation step introduces sulfonic groups and enhances thermal stability through cross-linking, while mechanical ball milling ensures uniform dispersion of KOH within the precursor. The fibrous mask structure was transformed into a highly porous carbon network with interconnected voids and a surface area of 601.6 $m^2 g^{-1}$ after the activation. The optimised sample delivers a high capacitance of 353 F g^{-1} at 1 A g^{-1} under a three-electrode configuration, and a symmetric device exhibits a capacitance of 122.6 F g^{-1} at 1 A g^{-1}, along with an energy density of 33.4 Wh kg^{-1} at 700 W kg^{-1} and good cycling stability (~82.6% retention after 10 000 cycles). Heteroatom doping, combined with intrinsic structural preservation, offers a distinct strategy to improve electrochemical performance while simplifying electrode fabrication. Ma and Zhao reported that nitrogen-doped integrated carbon sheets (X-CAC) were directly derived from waste leather *via* high-temperature carbonisation (900 °C) followed by CO_2 activation, enabling the simultaneous development of hierarchical porosity and retention of nitrogen functionalities from protein-rich precursors.[114] Unlike conventional powder-based carbons, the natural collagen fibre network of leather is preserved during carbonisation, forming a self-supported, binder-free, integrated electrode structure that inherently improves electron transport and avoids pore blockage. The optimised sample (SL-CAC) achieves a specific surface area of 748 $m^2 g^{-1}$ and a pore volume of 0.71 $cm^3 g^{-1}$, with a high mesopore fraction (~69%), which significantly enhances ion transport. It delivers a specific capacitance of 197.6 F g^{-1} at 0.3 A g^{-1} under a three-electrode configuration, whereas the device exhibits a specific capacitance of 183.2 F g^{-1} at a current density of 0.5 A g^{-1} as well as an energy density of 6.38 Wh kg^{-1} at a power density of 125.5 W kg^{-1}. A 3D honeycomb-like porous network with interconnected micro-, meso-, and macropores was prepared from agricultural wheat straw *via* pyrolysis followed by KOH activation (750 °C), enabling the transformation of initially low-porosity biomass into a highly porous carbon framework.[115] The optimised electrode, with a surface area of 1093.46 $m^2 g^{-1}$ after activation, exhibits capacitances of 281 F g^{-1} at 0.5 A g^{-1}. In a symmetric configuration, the device delivers a capacitance of 119.5 F g^{-1} at a current density of 0.5 A g^{-1}, with a corresponding energy density of up to 16.58 Wh kg^{-1} at a power density of 249.74 W kg^{-1}.

It is essential to note that the above studies show that the electrochemical performance of waste-derived carbon materials is governed by the interplay among precursor chemistry, pore architecture, and charge transport dynamics, rather than by surface area alone. Based on the precursor source, biomass-derived precursors inherently provide hierarchical structures and intrinsic heteroatoms, which facilitate pore development and introduce pseudocapacitive contributions. However, their heterogeneous composition often results in irregular pore networks and limited electrical conductivity, leading to inconsistent performance under practical conditions. In contrast, plastic-derived carbons offer more uniform carbon frameworks and improved structural control, but typically require additional activation or doping to introduce porosity and electrochemical activity. Industrial waste-derived carbons can benefit from inorganic constituents that assist pore formation, yet they frequently suffer from impurity-related issues that compromise conductivity and long-term stability. An expanded discussion is provided under 3.1 below.

3.1 Pore structure and charge storage: evidence of the three-electrode to device gap

Recent studies on hierarchical porous waste-derived carbons have reported remarkably high electrochemical performance, particularly in three-electrode configurations, where specific capacitance values frequently exceed 300–500 F g^{-1} in aqueous electrolytes.[37] While these results highlight the intrinsic charge-storage capability of such materials, a consistent discrepancy emerges when these systems are evaluated under practical two-electrode conditions, where significantly lower capacitance is typically observed. This divergence is not an isolated phenomenon but a recurring trend across a wide range of biomass- and waste-derived carbons, regardless of precursor type or synthesis strategy. A critical examination of the studies summarised in Table 2 reveals that materials exhibiting ultrahigh surface areas and excellent half-cell performance do not necessarily deliver comparable device-level behaviour. This mismatch arises from fundamental limitations associated with pore accessibility, ion transport, electrolyte compatibility, and internal resistance, which are largely suppressed under idealised three-electrode conditions. Consequently, the apparent superiority of many reported materials often reflects testing methodology rather

Table 2 Representative electrochemical performance of waste-derived porous carbons: comparison between three-electrode (intrinsic) and two-electrode (device-level) evaluation

S/No	Source of the waste	Surface area ($m^2\ g^{-1}$)	Pore structure	3-Electrode specific capacitance (F g^{-1} @ A g^{-1})	2-Electrode specific capacitance (F g^{-1} @ A g^{-1})	Energy density (Wh kg^{-1})@power density (W kg^{-1})	Gap factor	Ref.
1	Vinegar residue	2133.7	(Micro–meso)	351@0.5	62.4@0.5	10.5@275		96
2	Tea leaves	1001	Micro-meso	—	282@0.9	28.3@35		75
3	Husk of physalis	1677.19	Micro–meso-macro	387.9@0.5	84.7@0.5	30@1100		72
4	Turnip waste	644.981	Micro–meso	—	218@1	24.86@712.65		97
5	Platanus fibers	1406	Micro-meso	318@0.5	252@0.1	7.04@22.66		98
6	Tea waste	853.42	Micro-meso	—	89.62@0.1	17.92@35.29		99
7	Bamboo waste	1192	Micro–meso	~386.6@0.2	110@0.2	15.2@179.9		101
8	Wood waste		Hierarchical	—	164@0.5	61.19@23 220		74
	Coconut husk		Micro-meso	539.5@0.5	129.87@0.5	40.5@7500		100
9	Sawdust	1151	Micro–meso	~220 @ 0.1	—	—		102
10	Sugarcane bagasse	2455.6	Micro–meso	405.67@0.2	220.6@0.2	54.73@207.8		10
11	Five-eyed kernel	1475.36	Micro–macro	414.38@1	49.2@1	13.4@700		36
12	Cow urine	2651.7	Micro-meso	—	165@0.5	22.9@5100		26
13	Spiral algae/Industrial waste	1911.87	Micro-meso-macro	344.65@0.5	268.35@0.25	14.16@75		42
14	Coconut bract	767.3	Microporous	338@2	105@1	28.58@6997.72		103
15	Broad bean husk	2078.4	Micro-macro	386 @ 0.5	283.3@0.5	28.4@275		104
16	Sawdust	2072	Micro–meso	284@0.5	52@0.5	6.89@290.78		105
17	Tea saponin	1727	Tuned pores	388@0.5	187@0.5	43.9@1275		106
18	Corn bracts	286.5	Hierarchical	160.1@1	41.4@1	10.5@350		107
19	#Bird feather	763	Micro-meso	—	~384@1	13@250		108
20	#*Setaria viridis* stalks	1555.36	Micro-meso	~350@1	487@2	8.28@3500		109
21	Kish graphite waste	235.9	Micro–meso	—	85.3@0.1 mA g^{-1}	7.7@97		110
22	Rice husk	341.73	Micro-meso	—	58@0.1	—		111
23	Pineapple stem starch	2796	Micro-dominant	374 @0.1	37@0.1	5@49		58
24	Pyrolysed carbon black	622.9	Micro-meso	246@1	100@1	28.4@710		112
25	Kiwi	2691.85	Micro-meso	323.5@1	118.5@1	31.8@697		52
26	#*Murraya koenigii* seeds	798	Micro-meso	—	178.98@0.5 mA cm^{-2}	16.32@436		77
27	Red pepper industrial waste	1120.96	Micro–meso	—	4.59@0.015	0.102@3000		21
28	Chrysanthemum stems waste	1710.8	Micro-meso	366.5@0.5	272.9@0.5	18.7@325		113
29	#Medical waste	601.6	Micro–meso	353@1	122.6@1	33.4@700		3
30	Leather waste	748	Multi-scale	197.6@0.3	183.20.5	6.38@125.5		114
31	Wheat straw	1093.46	Microporous	281@0.5	119.5@0.5	16.58@249.74		115

than true device performance. On the other hand, pore structure is widely regarded as the primary determinant of charge storage in carbon-based supercapacitor electrodes, with micropores, mesopores, and macropores traditionally assigned distinct roles in capacitance and ion transport. Under idealised three-electrode conditions, micropores are often considered highly effective due to their large surface area, which enables substantial charge accumulation and leads to the frequently reported high capacitance values of 300–500 F g^{-1}. However, a closer comparison of the studies summarised in Table 2 reveals that this interpretation does not hold under practical two-electrode conditions. Across multiple systems, materials dominated by microporosity consistently exhibit a pronounced reduction in capacitance when evaluated at the device level, despite their exceptional intrinsic performance. This discrepancy indicates that the conventional understanding of pore-function relationships, largely derived from half-cell measurements, is insufficient to explain real device behaviour. In particular, factors such as limited ion accessibility, pore connectivity, electrolyte-dependent transport, and internal resistance fundamentally alter the contribution of different pore regimes. Therefore, rather than treating pore structure as a static descriptor of performance, it must be understood as a dynamic parameter whose effectiveness depends on operating conditions and device architecture. The following discussion critically examines how different pore structures influence charge storage and why their roles shift as the evaluation moves from idealised models to practical supercapacitor devices.

3.1.1 Micropore-dominated carbons: high capacitance, poor device translation. Micropore-dominated carbons represent one of the most widely reported classes of waste-derived electrode materials, primarily due to their exceptionally high specific surface areas and correspondingly high capacitance in three-electrode configurations. As summarised in Table 2, many of these materials exhibit gravimetric capacitance values exceeding 300–400 F g^{-1} when evaluated in half-cell systems. However, a consistent, systematic decline in performance is observed when these materials are translated into two-electrode devices, with capacitance values frequently falling below ~100–150 F g^{-1}. This discrepancy highlights a fundamental limitation of micropore-dominated architectures: high intrinsic capacitance does not necessarily translate into high device-level performance. For instance, starch-derived activated carbon (SAC-800), characterised by an ultrahigh surface area of approximately 2796 m^2 g^{-1} and a predominantly microporous structure, delivers a high capacitance of 374 F g^{-1} at low current density in a three-electrode configuration (Table 2). However, when assembled into a symmetric two-electrode device, the capacitance decreases drastically to approximately 37 F g^{-1} under comparable conditions. A similar pattern is observed for nitrogen- and sulfur-co-doped sugarcane bagasse-derived carbon (NS-WSB-AC), which exhibits a three-electrode capacitance of ~405.7 F g^{-1} but only ~220.6 F g^{-1} in a two-electrode asymmetric device. Likewise, five-eyed kernel-derived carbon (FKC-800) exhibits a capacitance of ~414.4 F g^{-1} in a three-electrode system, whereas its symmetric-device capacitance drops to ~49.2 F g^{-1} (Table 2). These examples demonstrate that the reduction is not incidental but rather an intrinsic characteristic of micropore-dominated systems. The origin of this behaviour lies in the limited accessibility of ultramicropores under practical operating conditions.[116] While micropores (<2 nm) contribute significantly to charge storage due to their high surface area, their effective utilisation is strongly dependent on ion transport dynamics.[117] In three-electrode configurations, the thin-electrode geometry and low mass loading facilitate sufficient ion diffusion into the confined pores, enabling near-complete utilisation of the internal surface area. However, in two-electrode devices, particularly at higher mass loadings and realistic current densities, ion transport into sub-nanometer pores becomes kinetically constrained.[118] As a result, a substantial fraction of the microporous surface remains electrochemically inactive within the timescale of operation.[119]

This limitation is further exacerbated by the nature of the electrolyte and the size of the solvated ion, as discussed in previous sections. In aqueous electrolytes, smaller hydrated ions can partially access micropores, allowing for relatively higher utilisation.[120] In contrast, in organic or ionic liquid electrolytes commonly used in practical devices, larger ion sizes and slower diffusion kinetics significantly restrict access to these narrow pores.[121] Consequently, materials that perform exceptionally well in aqueous three-electrode systems often exhibit pronounced performance degradation in two-electrode configurations. Another contributing factor is the structural disorder introduced during aggressive activation processes used to generate high microporosity. While chemical activation (*e.g.*, KOH treatment) effectively increases surface area, it also disrupts graphitic domains, thereby reducing electrical conductivity.[122] This introduces additional resistance within the electrode, further limiting charge propagation and reducing effective capacitance in full-cell systems. Thus, the combination of poor ion accessibility and reduced electronic conductivity creates a dual bottleneck that impairs device-level performance. Table 2 suggests that the magnitude of the capacitance reduction varies with the degree of microporosity and structural balance. Materials with extremely high surface areas dominated by ultramicropores tend to exhibit the largest drop when transitioning from three-electrode to two-electrode systems. In contrast, materials with a more balanced pore-size distribution exhibit better capacitance retention, indicating that accessibility and connectivity are more critical than absolute surface area.

3.1.2 Mesopore-rich architectures: improved rate capability. In contrast to micropore-dominated carbons, materials enriched with mesopores (2–50 nm) exhibit a more balanced and reliable translation of electrochemical performance from three-electrode to two-electrode systems. Although such materials typically have lower total surface areas than highly microporous carbons, their enhanced pore accessibility and improved ion-transport kinetics enable more effective utilisation of the active surface under practical operating conditions. As a result, mesopore-rich architectures often demonstrate superior rate capability and reduced performance loss during device-level evaluation. Evidence from Table 2

supports this trend. For example, tea-leaf-derived carbon activated *via* a combined $ZnCl_2/CO_2$ strategy exhibits a hierarchical structure with a significant mesoporous contribution and a moderate surface area of approximately 1001 m^2 g^{-1}. This material delivers a capacitance of ~282 F g^{-1} in a three-electrode configuration and retains a relatively high value of ~282 F g^{-1} in a symmetric two-electrode device at comparable current densities (Table 2). Similarly, $KMnO_4$-activated Platanus-fibre-derived carbon (OPF-700-3), which contains a well-developed micro-mesoporous network, shows a three-electrode capacitance of ~318 F g^{-1} and maintains ~252 F g^{-1} in a two-electrode configuration (Table 2). These examples show significantly smaller drops in capacitance than in micropore-dominated systems, indicating improved translation efficiency. The enhanced performance of mesopore-rich carbons can be attributed primarily to reduced ion diffusion resistance. Mesopores serve as transport channels that facilitate rapid electrolyte penetration and shorten diffusion pathways within the electrode.[122–124] Unlike ultramicropores, which impose steric and kinetic constraints on ion movement, mesopores provide sufficient space for solvated ions to move freely, even at high current densities.[125] This ensures that a larger fraction of the internal surface area remains accessible during fast charge–discharge cycles, thereby improving rate capability. This effect becomes particularly important in practical two-electrode devices, where electrodes are thicker, and mass loading is higher. Under such conditions, ion transport limitations become a dominant factor controlling performance. Mesoporous networks mitigate these limitations by acting as ion-buffering reservoirs, enabling uniform ion distribution throughout the electrode and reducing concentration gradients.[126] Consequently, mesopore-rich materials exhibit better capacitance retention across a wide range of current densities, as reflected in their relatively stable two-electrode performance. Another advantage of mesoporous structures is their compatibility with a wider range of electrolytes. As discussed earlier, larger solvated ions in organic and ionic liquid electrolytes often struggle to access narrow micropores. Mesopores, by contrast, can accommodate these ions more readily, ensuring effective charge storage even in non-aqueous systems. This makes mesopore-rich carbons more suitable for practical applications that require higher operating voltages and energy densities.[127] However, it is important to note that mesoporosity alone does not guarantee superior performance. Excessive mesopore content can reduce surface area and, consequently, overall capacitance. This trade-off is evident in some materials listed in Table 2, where moderate surface areas combined with mesoporous structures yield stable but not exceptionally high capacitance values. Therefore, while mesopores enhance ion transport, they must be integrated with an adequate proportion of micropores to maintain sufficient charge storage capacitance. Additionally, the effectiveness of mesopores depends on their connectivity and distribution within the carbon matrix.[127] Isolated or poorly connected mesopores may not contribute significantly to ion transport, whereas well-interconnected networks can dramatically improve electrolyte accessibility. Thus, the design of mesopore-rich carbons must consider not only pore size but also pore architecture and connectivity.

3.1.3 Role of heteroatom doping: real gains *vs.* overstated effects. Heteroatom doping has become a widely adopted strategy for enhancing the electrochemical performance of waste-derived carbon materials. Incorporation of elements such as nitrogen, sulfur, phosphorus, and boron is often reported to improve capacitance through multiple mechanisms, including increased surface wettability, enhanced electrical conductivity, and the introduction of pseudocapacitive redox-active sites.[128,129] However, a critical comparison of studies summarized in Table 2 reveals that the benefits of heteroatom doping are frequently overstated, particularly when evaluated in the context of practical two-electrode devices. Several doped carbon systems demonstrate high capacitance in three-electrode configurations, often exceeding 350–500 F g^{-1}. For example, boron-doped nanocarbon derived from coconut husk exhibits an exceptionally high capacitance of ~539.5 F g^{-1} in a three-electrode system, whereas the corresponding two-electrode device capacitance is ~129.9 F g^{-1} (Table 2). Similarly, nitrogen-doped porous carbon derived from Physalis calyx (NPPCPC-1) delivers ~387.9 F g^{-1} in three-electrode testing but only ~84.7 F g^{-1} in a symmetric device (Table 2). These examples indicate that although doping can enhance intrinsic capacitance, it does not necessarily translate into proportional improvements at the device level. A key reason for this discrepancy is that the apparent performance enhancement attributed to doping is often coupled with changes in pore structure rather than arising solely from electronic effects. In many synthesis routes, doping occurs simultaneously with activation, thereby modifying the pore size distribution, increasing defect density, and altering surface functionality.[130,131] As a result, it becomes difficult to isolate the true contribution of heteroatoms from that of structural changes. In some cases, the observed increase in capacitance may be primarily driven by improved porosity or accessibility rather than by pseudocapacitive effects. Moreover, the contribution of heteroatom-induced pseudocapacitance is often limited under practical conditions. While redox-active functional groups can enhance capacitance in three-electrode systems, particularly at low scan rates or current densities, their effectiveness diminishes at higher rates due to kinetic constraints. In two-electrode devices, where rapid charge–discharge is required, the contribution from surface redox reactions may be significantly reduced, leading to a smaller-than-expected improvement in overall performance. The impact of doping on electrical conductivity also presents a nuanced picture.[132] Nitrogen doping, for instance, can improve conductivity by introducing electron-donating sites and increasing charge-carrier density. This can facilitate faster electron transport and partially compensate for the loss of conductivity associated with high porosity. However, excessive doping or the introduction of certain heteroatoms can increase structural disorder, disrupt graphitic domains, and negatively affect conductivity.[133] This trade-off is evident in several materials listed in Table 2, where doped carbons with high defect density do not outperform their less-doped or undoped counterparts in device configurations.

Co-doping strategies (*e.g.*, N/S or N/P) have been proposed to create synergistic effects by combining multiple functionalities. For example, N, S-codoped carbon derived from sugarcane bagasse exhibits a relatively high two-electrode capacitance ($\sim$220.6 F g^{-1}) compared to many other systems (Table 2). This suggests that, under certain conditions, doping can meaningfully enhance performance when combined with favourable pore architecture and good conductivity. However, such improvements are not universal and depend strongly on the specific synthesis method, dopant concentration, and resulting structural features. Another important consideration is the stability of doped functional groups. While heteroatoms can introduce additional active sites, these sites may not be stable over prolonged cycling, particularly in harsh electrolytes or at high potentials.[134] Degradation of functional groups can lead to capacitance fading, thereby reducing the device's long-term performance. This effect is often overlooked in studies that focus primarily on initial capacitance values.

3.1.4 Hierarchical structures: when do they actually work? Hierarchical porous carbons, comprising an integrated network of micropores, mesopores, and macropores, are widely regarded as an optimal structural design for supercapacitor electrodes.[57,122] In principle, such architectures combine the advantages of each pore regime: micropores provide a high surface area for charge storage, mesopores facilitate ion transport, and macropores act as ion-buffering reservoirs that enhance electrolyte diffusion. However, a critical evaluation of the data presented in Table 2 reveals that the effectiveness of hierarchical structures is not universal. Instead, their performance depends strongly on pore connectivity, structural balance, and the degree of functional integration across different pore scales. Several examples from Table 2 demonstrate that well-designed hierarchical carbons can achieve improved translation from three-electrode to two-electrode systems. For instance, nitrogen-doped porous carbon derived from Physalis calyx (NPPCPC-1), featuring a micro-meso-macroporous structure with a surface area of $\sim$1677 m^2 g^{-1}, delivers a capacitance of $\sim$387.9 F g^{-1} in a three-electrode configuration and retains $\sim$84.7 F g^{-1} in a symmetric two-electrode device (Table 2). Similarly, bamboo-derived NP(1 : 1)-HPC with hierarchical porosity exhibits a three-electrode capacitance of $\sim$386.6 F g^{-1} and a device capacitance of $\sim$110 F g^{-1}. Compared with purely microporous systems, these materials exhibit improved capacitance retention, reflecting the beneficial role of meso- and macroporous channels in enhancing ion accessibility. Another notable example is the tea-saponin-derived porous carbon (TSUK-700), which combines micropores with interconnected mesoporous pathways.[106] This material delivers $\sim$388 F g^{-1} in a three-electrode configuration and maintains $\sim$187 F g^{-1} in a two-electrode configuration, representing a significantly smaller performance drop than micropore-dominated carbons. These results suggest that when hierarchical structures are properly engineered, they can effectively mitigate ion transport limitations and enable more efficient utilisation of the internal surface area. However, the data in Table 2 also indicate that not all hierarchical carbons achieve this level of performance. In some cases, materials classified as hierarchical still exhibit substantial capacitance losses when transitioning to two-electrode systems. For example, certain highly activated biomass-derived carbons with nominally hierarchical pore distributions exhibit large discrepancies between three-electrode and device performance, similar to micropore-dominated systems (Table 2). This suggests that the mere presence of multiple pore sizes is insufficient; rather, the connectivity and accessibility of these pores are the determining factors. A key limitation arises when micropores dominate the structure without sufficient mesoporous pathways to facilitate ion transport. In such cases, mesopores may be present but poorly interconnected, leading to high tortuosity and restricted electrolyte penetration.[52] As a result, ions cannot efficiently access deeper microporous regions, and the hierarchical advantage is effectively lost. Similarly, excessive activation can generate disordered pore networks with weak structural integrity, further reducing the effectiveness of hierarchical design. Another critical factor is the balance between porosity and conductivity. As discussed in the previous section, over-activation can disrupt graphitic domains and reduce electrical conductivity, thereby limiting charge propagation across the electrode. Even in hierarchical systems, insufficient conductivity can lead to localised polarisation and underutilization of active sites, diminishing overall performance.[26] The role of macropores is also often overstated. While macropores can serve as ion reservoirs and reduce diffusion distances, their contribution to capacitance is minimal due to their low surface area. If macroporosity is introduced at the expense of microporous surface area, the overall capacitance may decrease despite improved transport properties. Therefore, an optimal hierarchical structure requires a carefully tuned balance between pore sizes, ensuring that macropores and mesopores enhance accessibility without significantly compromising charge storage capacitance.[8]

Indeed, Table 2 indicates that hierarchical structures are effective only when they satisfy three key conditions: (i) continuous and well-connected pore networks that enable efficient ion transport, (ii) an appropriate balance between micropores and mesopores to maximise both storage and accessibility, and (iii) sufficient electrical conductivity to support rapid electron transfer. When these conditions are met, hierarchical carbons can significantly reduce the performance gap between three-electrode and two-electrode systems. Conversely, when these conditions are not fulfilled, hierarchical labelling alone does not guarantee improved device performance. It is worth noting that an important parameter that significantly influences the reported electrochemical performance but is often overlooked in comparative analyses is the mass loading of the active material. In many studies, high specific capacitance values are obtained at very low mass loadings (typically $\leq$1–2 mg cm^{-2}), thereby facilitating rapid ion transport and maximising surface utilisation.[66] However, such conditions do not accurately reflect practical device configurations, where higher mass loadings are required to achieve meaningful energy density. As electrode thickness increases, ion-diffusion limitations, pore-accessibility constraints, and internal resistance become more pronounced, leading to

a substantial reduction in effective capacitance.[135] It is noteworthy that, among the studies summarised in Table 2, only a very limited number explicitly report the mass loading of the active material (indicated by "#"), while the majority of the literature does not provide this critical parameter. This lack of reporting complicates direct comparison across studies and further contributes to the overestimation of electrochemical performance, particularly in three-electrode evaluations.

4. Design principles for bridging lab-scale performance to practical devices

The analysis of structure–performance relationships and the persistent discrepancy between three-electrode and two-electrode results clearly indicate that current research on waste-derived carbon materials remains largely biased toward intrinsic material optimisation rather than device-oriented design. As highlighted throughout Section 3, materials exhibiting exceptionally high capacitance in three-electrode systems often fail to deliver comparable performance in practical devices due to limitations in ion transport, pore accessibility, and internal resistance. Therefore, bridging this gap requires a shift from maximising isolated parameters to adopting integrated design principles that reflect realistic operating conditions.

4.1 Optimising pore size distribution for accessible charge storage

A fundamental requirement for improving device-level performance is the rational design of pore size distribution. While micropores are essential for charge storage due to their high surface area, their effectiveness is limited by accessibility constraints, particularly in thick electrodes and at high current densities. As discussed earlier, many materials reported exhibit high three-electrode capacitance (>300–400 F g^{-1}) but significantly lower device capacitance due to limited utilisation of micropores. Evidence from hierarchical carbons such as NPPCPC-1 and bamboo-derived NP(1 : 1)-HPC demonstrates that integrating mesopores with micropores improves ion transport and enhances device-level capacitance (Table 2). Mesopores provide pathways for electrolyte diffusion, enabling more effective utilisation of microporous surfaces. Therefore, optimal design should prioritise accessible surface area rather than total surface area, ensuring that a significant fraction of the pore network participates in charge storage under practical conditions.

4.2 Balancing surface area and electrical conductivity

Another critical design consideration is the trade-off between porosity and electrical conductivity. Aggressive activation strategies, such as KOH activation, are widely used to generate high surface areas but often result in highly disordered carbon structures with reduced conductivity. This structural disorder limits electron transport, particularly in thick electrodes, thereby increasing internal resistance and reducing effective capacitance. Several examples in Section 3, illustrate that materials with moderate surface areas but improved conductivity can outperform highly porous carbons at the device level. For instance, graphite-integrated activated carbon composites demonstrate improved conductivity and more stable performance despite lower surface areas (Table 2). Similarly, nitrogen-doped graphite-like carbon structures exhibit enhanced charge transport due to partial graphitisation. These observations suggest that maintaining continuous conductive pathways is essential for efficient charge propagation and overall device performance.

4.3 Engineering electrodes for high mass loading and thickness

Most three-electrode evaluations are conducted at low mass loadings, thereby facilitating rapid ion transport and maximising apparent capacitance. However, practical devices require significantly higher mass loadings to achieve meaningful energy densities. As electrode thickness increases, ion diffusion becomes increasingly limited, leading to incomplete utilisation of the active material. The importance of this effect is evident in several examples discussed in Table 2, where materials exhibiting high capacitance in thin electrodes show substantial performance degradation in two-electrode configurations. In contrast, studies that incorporate realistic electrode architectures, such as cylindrical 18 650-type configurations, demonstrate more representative performance but often with reduced capacitance due to transport limitations.[65,66] To address this challenge, electrode design must focus on reducing diffusion resistance through hierarchical pore networks, improving electrolyte penetration, and minimising tortuosity. Additionally, optimising electrode fabrication parameters, such as packing density and binder content, is essential for maintaining structural integrity while preserving pore accessibility.

4.4 Matching electrolyte properties with pore architecture

The compatibility between electrolyte characteristics and pore structure is a key determinant of performance translation. Indeed, aqueous electrolytes enable high capacitance due to their high ionic conductivity and small ion sizes, but they are limited by narrow voltage windows.[121] In contrast, organic and ionic liquid electrolytes enable higher operating voltages but impose limitations due to larger ion sizes and slower diffusion kinetics.[116,136] This mismatch is particularly critical for micropore-dominated carbons, where a large fraction of the surface area may be inaccessible to bulky ions. As a result, materials optimised for aqueous systems often exhibit reduced performance when used in practical devices employing non-aqueous electrolytes. Therefore, the pore size distribution must be tailored to the specific electrolyte system to ensure that ion accessibility is maintained under realistic conditions.

4.5 Rational use of heteroatom doping

Heteroatom doping is frequently employed to enhance electrochemical performance by introducing additional active sites and improving wettability. Section 3.1 provides multiple examples of doped carbons exhibiting high capacitance in

three-electrode systems, such as boron-doped carbon (~539.5 F g^{-1}) and nitrogen-doped porous carbons (>380 F g^{-1}). However, the corresponding improvements in two-electrode devices are often less pronounced, indicating that doping alone does not guarantee enhanced device performance. In many cases, the benefits attributed to doping are intertwined with changes in pore structure and activation conditions. Furthermore, excessive doping can introduce structural defects that negatively affect conductivity and stability. Therefore, doping should be considered a complementary strategy that enhances performance when combined with optimised pore architecture and conductivity, rather than a primary design objective.

4.6 Minimising internal resistance and enhancing charge transport

Internal resistance is a critical factor limiting the performance of practical supercapacitors. Equivalent series resistance (ESR) arises from the combined contributions of electrolyte resistance, electrode conductivity, and interfacial contact resistance.[137] High ESR leads to voltage drops during charge–discharge cycles, reducing both power and energy density. Materials with highly disordered structures or poor conductivity often exhibit higher ESR, which limits their practical applicability. Strategies to minimise resistance include enhancing graphitic ordering, improving electrode–current collector interfaces, and optimising electrolyte infiltration. Additionally, maintaining a balance between porosity and structural integrity is essential to avoid excessive resistance associated with over-activation.

5. Practical limitations and scalability of waste-derived carbons in supercapacitors

Despite the strong interest in waste-derived carbons as sustainable electrode materials, their practical deployment is constrained by yield, cost, reproducibility, and environmental impact. While the use of biomass or waste precursors is inherently attractive from a resource perspective, the overall feasibility of these materials is dictated primarily by the processing routes required to achieve high electrochemical performance.[6] For instance, chemical activation, particularly using KOH, remains the most widely adopted method due to its ability to generate ultrahigh surface areas and high capacitance in three-electrode systems. However, this approach is inherently inefficient in terms of scalability. Severe chemical etching leads to low carbon yield, while the high consumption of activating agents, often in excess of the precursor mass, significantly increases cost and produces large volumes of chemical waste. In addition, extensive post-treatment using acids and water is required to remove residual species, further amplifying environmental burden and process complexity.[16] Although $ZnCl_2$ activation offers relatively higher yield and promotes mesoporous structures, its toxicity, corrosiveness, and waste management challenges limit its industrial applicability. In response, greener activation strategies, such as K_2CO_3 or $KHCO_3$ treatment and physical activation with CO_2 or steam, have been explored to reduce chemical consumption and environmental impact. These methods improve process sustainability and simplify production but typically result in lower surface areas and require further optimisation to achieve comparable electrochemical performance. At the same time, the high temperatures required for carbonisation and activation (typically 700–900 °C) impose substantial energy demands, increasing both production cost and carbon footprint.[6,135] Multi-step synthesis routes further compound this issue, highlighting the need for simplified and energy-efficient processing. Beyond processing constraints, the intrinsic variability of biomass precursors presents a major challenge to reproducibility. Unlike synthetic materials, biomass exhibits significant compositional heterogeneity, including variations in lignin, cellulose, hemicellulose, and naturally occurring heteroatoms.[9] These differences directly influence carbonisation behaviour, pore development, and final material properties. Even under identical synthesis conditions, such variability can lead to substantial batch-to-batch differences in surface area, pore structure, and conductivity. This inconsistency is further amplified during chemical activation, where precursor-dependent interactions result in unpredictable structural evolution and material yield. The widespread performance metrics reported for similar biomass sources reflect this issue and complicate both comparison across studies and scale-up efforts. Environmental feasibility also requires careful consideration. The assumption that waste-derived carbons are inherently "green" is not valid when the full lifecycle of the process is examined. High chemical consumption, water-intensive purification, and energy-demanding thermal treatments can offset the environmental benefits of using waste feedstocks.[11] Moreover, low carbon yield and inefficient resource utilisation can undermine the sustainability claims of such materials. Without proper recovery and recycling of chemicals, these processes may introduce additional environmental risks rather than mitigating existing ones. From an industrial perspective, scalability is further limited by the complexity and sensitivity of current synthesis methods. Laboratory-scale processes often rely on batch operations with tightly controlled conditions, which are difficult to replicate in continuous manufacturing systems.[135] Maintaining consistent product quality becomes particularly challenging in the presence of precursor variability and process-dependent structural evolution.

Overall, the transition of waste-derived carbons from laboratory research to practical applications requires a shift toward process-efficient, reproducible, and environmentally responsible synthesis strategies. This includes reducing chemical consumption, improving carbon yield, minimising energy input, and developing robust methods that can accommodate precursor variability. Without addressing these fundamental limitations, the widespread adoption of waste-derived carbon materials in commercial supercapacitors will remain constrained despite their promising laboratory performance.

6. Future outlook

The analysis presented in this review demonstrates that the primary barrier to the practical implementation of waste-

derived carbon electrodes is not the lack of high surface area or advanced pore engineering, but the mismatch between intrinsic material evaluation and realistic device operation. In particular, factors such as low mass loading, limited ion accessibility in thick electrodes, and internal resistance collectively contribute to the substantial performance gap observed between three-electrode and two-electrode systems.[135] Therefore, future development must move beyond maximising intrinsic capacitance and instead prioritise device-relevant design criteria. This includes (i) engineering pore structures that maintain ion accessibility under high mass loading conditions, (ii) optimising electrode thickness and packing density to minimise diffusion limitations and resistive losses, and (iii) integrating conductive networks to mitigate internal resistance in practical configurations. In addition, the inconsistent reporting of key parameters, such as mass loading and voltage window, highlights the urgent need for standardised evaluation protocols to enable meaningful comparisons across studies. From a translational perspective, scalable synthesis routes must be aligned with electrode fabrication strategies to ensure that laboratory-scale materials can be effectively implemented in full-cell architectures.[66] Without this integration, improvements in specific capacitance observed under idealised conditions are unlikely to translate into reliable device performance. Ultimately, advancing waste-derived carbon materials toward commercial supercapacitor applications requires a paradigm shift from reporting peak laboratory metrics to establishing reproducible, standardised, and device-relevant performance benchmarks. Achieving this goal requires adopting specific methodological and reporting practices. First, electrochemical performance should be evaluated under realistic conditions, including mass loadings above 5–10 mg cm^{-2}, appropriate electrode thickness, and full two-electrode device configurations.[65] Second, both three-electrode and two-electrode data should be reported concurrently to enable meaningful comparison and avoid performance overestimation. Third, key parameters such as mass loading, voltage window, and internal resistance must be consistently disclosed to ensure reproducibility. In addition, electrode design should prioritise pore accessibility and conductive pathways that remain effective under practical operating conditions, rather than optimising surface area alone. Finally, benchmarking against commercially available devices, rather than solely against literature values, is essential for evaluating real-world applicability.[135] These approaches provide a practical pathway for transitioning from record-high laboratory metrics to reliable and scalable device performance. From a characterisation perspective, future studies should move beyond conventional surface area analysis and incorporate techniques that directly probe ion transport and pore accessibility under operating conditions. In particular, EIS should be employed more systematically to evaluate frequency-dependent behaviour and the relaxation time (τ_0), thereby providing insight into charge propagation dynamics. *In situ* and *operando* techniques, such as *in situ* Raman spectroscopy, X-ray diffraction, and electrochemical quartz crystal microbalance (EQCM), can further elucidate ion adsorption, structural evolution, and electrolyte interactions within porous carbon frameworks. Additionally, advanced pore characterisation methods, including density functional theory (DFT) analysis of adsorption isotherms and small-angle scattering techniques, are essential for accurately resolving micro-mesopore distributions and their accessibility to electrolyte ions.

7. Conclusion

Over the past decade, significant progress has been made in the development of waste-derived porous carbons for supercapacitor applications, particularly in terms of increasing specific surface area, tuning hierarchical pore structures, and introducing heteroatom functionalities. Early studies primarily focused on maximising microporosity to enhance electric double-layer capacitance, often achieving surface areas exceeding 1000 m^2 g^{-1}.[15,16] As highlighted above, more recent works have demonstrated that incorporating mesopores and macropores improves ion transport kinetics and rate capability, thereby enhancing performance at high current densities. In addition, heteroatom doping (*e.g.*, N, S, P, B) has emerged as an effective approach to enhance wettability, electrical conductivity, and pseudocapacitive contributions, thereby improving electrochemical performance relative to undoped carbons. Recent studies have also explored integrated synthesis approaches that combine activation, doping, and partial graphitisation to balance porosity and conductivity.[14] Indeed, this review shows that their performance is often overestimated under three-electrode conditions. A systematic gap exists between intrinsic capacitance and device-level performance, arising from ion transport limitations, restricted pore accessibility, electrolyte mismatch, and internal resistance. Comparative analysis reveals that ultrahigh surface area alone does not guarantee superior performance. Micropore-dominated carbons, despite delivering >300–500 F g^{-1} in three-electrode systems, frequently exhibit significant losses in two-electrode devices due to poor accessibility and slow diffusion. In contrast, balanced micro–mesoporous architectures provide more reliable performance translation, emphasising the importance of accessible porosity over total surface area. Similarly, the benefits of hierarchical structuring and heteroatom doping are conditional and depend on pore connectivity and conductivity rather than their mere presence. The performance gap is further amplified by non-standardised evaluation practices, including low mass loading, limited voltage windows, and neglect of internal resistance, which collectively lead to inflated metrics. Addressing this requires a shift toward device-relevant testing protocols and consistent reporting standards.

Author contributions

Mustapha Balarabe Idris: conceptualization, data curation, formal analysis, investigation, validation, writing and editing. Bhekie B. Mamba: editing, funding acquisition, project administration, Fuku Xolile: editing, funding acquisition, project administration, resources, supervision, visualization, writing – review & editing.

Conflicts of interest

The authors declare that they have no known competing financial interests or personal relationships that could have appeared to influence the work reported in this paper.

Data availability

Data will be made available on request.

Acknowledgements

The authors would like to express their gratitude to the University of South Africa, the Institute for Nanotechnology and Water Sustainability (iNanoWS), College of Science, Engineering, and Technology for funding and research facilities. During the preparation of this work, the author(s) used Grammarly software for spelling, grammar, and punctuation checks. Gemini AI is also used for image generation. After using these tools, the author(s) reviewed and edited the content as needed and take(s) full responsibility for the content of the published article.

References

1 M. B. Idris, Z. Musa Mohammed, S. Nuhu, H. Aliyu, H. Abba, B. B. Mamba, D. Sappani and F. Xolile, Recent Advances in Mesoporous Carbon Nitride-Based Materials for Electrochemical Energy Storage and Conversion and Gas Storage, *ACS Omega*, 2025, **10**, 18184–18212.

2 G. Arumugam, B. Chettiannan, S. Mathan, M. Selvaraj, M. A. Assiri and R. Rajendran, Better understanding of redox additives in aqueous electrolyte for electrochemical supercapacitors, *J. Energy Storage*, 2025, **121**, 116595.

3 X. Ma, Z. Fan, M. Liu, Y. Cui, H. Ni, Y. Wu, Q. Sun, B. Fu and J. Wang, From medical waste to energy storage: Sulfonation-ball-milling derived porous carbon from waste masks for high-performance supercapacitors, *Sustain. Mater. Technol.*, 2026, **47**, e01890.

4 M. B. Idris, G. Sakthivel and S. Devaraj, Textural properties dependent supercapacitive performances of mesoporous graphitic carbon nitride, *Mater. Today Energy*, 2018, **10**, 325–335, DOI: 10.1016/j.mtener.2018.10.012.

5 E. Yildiz, S. Yasa, G. Ozsin and M. Gencten, Upcycling pyrolysis fuel oil into high-performance carbon electrodes for sustainable symmetric supercapacitors, *Sustain. Mater. Technol.*, 2025, **45**, e01510.

6 S. Ruan, X. He, H. Huang, Y. Gan, Y. Xia, J. Zhang, W. Wan, C. Wang, X. Xia and W. Zhang, Innovative approaches of porous carbon materials derived from energy waste and their electrochemical properties, *Energy Mater.*, 2025, **5**, 500066.

7 M. Fu, J. Huang, S. Feng, T. Zhang, P.-C. Qian and W.-Y. Wong, One-step solid-state pyrolysis of bio-wastes to synthesize multi-hierarchical porous carbon for ultra-long life supercapacitors, *Mater. Chem. Front.*, 2021, **5**, 2320–2327.

8 X. Bai, Z. Wang, J. Luo, W. Wu, Y. Liang, X. Tong and Z. Zhao, Hierarchical porous carbon with interconnected ordered pores from biowaste for high-performance supercapacitor electrodes, *Nanoscale Res. Lett.*, 2020, **15**, 88.

9 P. Dzikunu, E. S. Appiah, E. K. Arthur, S. O. Akinwamide, E. Gikunoo, E. A. Fangnon, K. Mensah-Darkwa, A. Andrews and P. Vilaça, Waste-to-carbon-based supercapacitors for renewable energy storage: progress and future perspectives, *Mater. Renew. Sustain. Energy*, 2025, **14**, 8.

10 J. Singh, B. Dey, M. M. A. Alwi, S. K. S. Hossain, A. Choudhury, A. Niaz, H. Khan and D.-J. Yang, Waste biomass-derived N, S-codoped porous carbon flakes for high energy density asymmetric supercapacitors, *Solid State Sci.*, 2025, **168**, 108014.

11 J. Feng, Q. Zhu, Q. Le, W. Zhu, B. Song, Z. Zhang and J. C.-H. Lam, Source and performance of waste-derived porous carbon material as supercapacitor: Biomass, sludge and plastic waste as precursors, *Renew. Sustain. Energy Rev.*, 2025, **211**, 115178, DOI: 10.1016/j.rser.2024.115178.

12 P. Dzikunu, E. S. Appiah, E. K. Arthur, S. O. Akinwamide, E. Gikunoo, E. A. K. Fangnon, K. Mensah-Darkwa, A. Andrews and P. Vilaça, Waste-to-carbon-based supercapacitors for renewable energy storage: progress and future perspectives, *Mater. Renew. Sustain. Energy*, 2025, **14**, 8, DOI: 10.1007/s40243-024-00285-4.

13 S. Guo, D. Zhang, Y. Zhao, H. Qu, X. Li and Y. Shen, Recent progress in food waste-derived porous carbons for supercapacitors, *Green Chem.*, 2026, **28**, 1375–1412, DOI: 10.1039/D5GC05691H.

14 K. V. G. Raghavendra, C. V. V. Muralee Gopi, V. Narayanaswamy, S. Alzahmi, B. Issa and I. M. Obaidat, From waste to power: Advances in biomass-derived carbon materials for sustainable supercapacitor electrodes, *J. Energy Storage*, 2026, **156**, 121558, DOI: 10.1016/j.est.2026.121558.

15 N. P. D. Ngidi, A. F. Koekemoer and S. S. Ndlela, Recent advancement in the electrochemical performance of electrochemical capacitors based on biomass-derived porous carbon: A review, *J. Energy Storage*, 2024, **89**, 111638, DOI: 10.1016/j.est.2024.111638.

16 A. B. Gueye, S. John, M. Fall, V. S. Saji and S. Thomas, Recent advances in biowaste-based carbon materials for electrochemical energy storage applications, *J. Energy Storage*, 2025, **139**, 118646.

17 B. E. Conway, *Electrochemical Supercapacitors: Scientific Fundamentals and Technological Applications*, Springer Science & Business Media, 2013.

18 M. B. Idris, S. Nuhu, Z. M. Mohammed, H. Aliyu, H. Abba, F. Xolile and S. Devaraj, Progress in metal-organic frameworks and their carbon-based composites for supercapacitor, *J. Energy Storage*, 2024, **93**, 112322.

19 M. Gopika, A. Sudarsanan, K. Sreelatha and B. Saraswathyamma, A comprehensive review on advancements, challenges, and future possibilities of

biomass-derived porous carbon for supercapacitors, *Prog. Solid State Chem.*, 2026, 100572.
20 Y. Yin, Q. Liu, Y. Zhao, T. Chen, J. Wang, L. Gui and C. Lu, Recent progress and future directions of biomass-derived hierarchical porous carbon: Designing, preparation, and supercapacitor applications, *Energy Fuels*, 2023, **37**, 3523–3554.
21 S. N. Karademir and I. Inal, Electrochemical and Mechanical Characterization of Waste Biomass-Derived Activated Carbon-Modified Carbon Fiber Fabrics for Potential Structural Supercapacitors, *Waste Biomass Valor.*, 2026, 1–15.
22 M. B. Idris and S. Devaraj, Mesoporous graphitic carbon nitride synthesized using biotemplate as a high-performance electrode material for supercapacitor and electrocatalyst for hydrogen evolution reaction in acidic medium, *J. Energy Storage*, 2019, **26**, 101032, DOI: 10.1016/j.est.2019.101032.
23 X. Liu, S. Zhang, X. Wen, X. Chen, Y. Wen, X. Shi and E. Mijowska, High yield conversion of biowaste coffee grounds into hierarchical porous carbon for superior capacitive energy storage, *Sci. Rep.*, 2020, **10**, 3518.
24 D. Merum and M. Kang, From biomass to energy storage: sustainable carbon materials for next-generation supercapacitors, *Ind. Eng. Chem. Res.*, 2025, **1**, 26.
25 B. Liu, Y. Ye and T. Li, Biomass-derived porous carbon materials for supercapacitors, in: *Porous Carbon Mater. Clean Energy*, CRC Press, 2024: pp. 105–126.
26 N. P. Reddy, R. J. Naik, N. Macherla, D. P. Joseph, R. I. Jafri, C. H. Ahn, M. R. Siddiqui, V. Gonuguntla and S.-H. Park, Biowaste-derived hierarchical activated porous carbon with heteroatom-doping (N/S) for efficient symmetrical supercapacitors: A cow urine approach, *J. Energy Storage*, 2025, **115**, 115964.
27 D. Guo, X. Song, B. Li, L. Tan, H. Ma, H. Pang, X. Wang, L. Zhang and D. Chu, Oxygen enriched carbon with hierarchical porous structure derived from biomass waste for high-performance symmetric supercapacitor with decent specific capacity, *J. Electroanal. Chem.*, 2019, **855**, 113349.
28 K. Barta and P. C. Ford, Catalytic conversion of nonfood woody biomass solids to organic liquids, *Acc. Chem. Res.*, 2014, **47**, 1503–1512.
29 H. Ma, J. Yang, X. Gao, Z. Liu, X. Liu and Z. Xu, Removal of chromium (VI) from water by porous carbon derived from corn straw: Influencing factors, regeneration and mechanism, *J. Hazard. Mater.*, 2019, **369**, 550–560.
30 Z. Zhou, J.-P. Cao, Y. Wu, Q.-Q. Zhuang, X.-Y. Zhao, Y.-L. Wei and H.-C. Bai, Waste sugar solution polymer-derived N-doped carbon spheres with an ultrahigh specific surface area for superior performance supercapacitors, *Int. J. Hydrogen Energy*, 2021, **46**, 22735–22746.
31 J. Li, Z. Yu, X. Ma, X. Zhang and W. Yue, Co-pyrolysis of bamboo with low-dose guanidine phosphate to synthesis heteroatom-enriched porous carbon materials for supercapacitors, *J. Anal. Appl. Pyrolysis*, 2025, **189**, 107095.
32 M. Szkoda, M. Skorupska, J. P. Łukaszewicz and A. Ilnicka, Enhanced supercapacitor materials from pyrolyzed algae and graphene composites, *Sci. Rep.*, 2023, **13**, 21238.
33 V. Prabhin, V. Benitha, K. Jeyasubramanian, R. S. Selvakumari and D. Divakaran, Effective utilization and characterization of carbon derived from non-biodegradable waste based electrical switches for supercapacitor applications: a green approach, *Waste Biomass Valor.*, 2024, **15**, 709–725.
34 Q. Hou, M. Zhen, H. Qian, Y. Nie, X. Bai, T. Xia, M. L. U. Rehman, Q. Li and M. Ju, Upcycling and catalytic degradation of plastic wastes, *Cell Rep. Phys. Sci.*, 2021, **2**, 100514.
35 C. Schneidermann, P. Otto, D. Leistenschneider, S. Grätz, C. Eßbach and L. Borchardt, Upcycling of polyurethane waste by mechanochemistry: synthesis of N-doped porous carbon materials for supercapacitor applications, *Beilstein J. Nanotechnol.*, 2019, **10**, 1618–1627.
36 C. Han and D. Ma, From agri-waste to high-performance energy storage: Self-doped N/O-enriched porous carbon derived from five-eye kernels for sustainable supercapacitors, *Mater. Today Commun.*, 2025, **46**, 112938.
37 S. Sundriyal, V. Shrivastav, H. D. Pham, S. Mishra, A. Deep and D. P. Dubal, Advances in bio-waste derived activated carbon for supercapacitors: Trends, challenges and prospective, *Resour. Conserv. Recycl.*, 2021, **169**, 105548.
38 V. Chaturvedi, S. Usangonvkar and M. V. Shelke, Synthesis of high surface area porous carbon from anaerobic digestate and it's electrochemical study as an electrode material for ultracapacitors, *RSC Adv.*, 2019, **9**, 36343–36350.
39 X. Yuan, Y. Shen, P. A. Withana, O. Mašek, C. S. K. Lin, S. You, F. M. Tack and Y. S. Ok, Thermochemical upcycling of food waste into engineered biochar for energy and environmental applications: A critical review, *Chem. Eng. J.*, 2023, **469**, 143783.
40 D. R. Lobato-Peralta, P. U. Okoye and C. Alegre, A review on carbon materials for electrochemical energy storage applications: State of the art, implementation, and synergy with metallic compounds for supercapacitor and battery electrodes, *J. Power Sources*, 2024, **617**, 235140.
41 L. K. Shrestha, R. G. Shrestha, S. Shahi, C. L. Gnawali, M. P. Adhikari, B. N. Bhadra and K. Ariga, Biomass nanoarchitectonics for supercapacitor applications, *J. Oleo Sci.*, 2023, **72**, 11–32.
42 W. Yue, Z. Yu, X. Zhang, H. Liu, Z. Chen, J. Chen, H. Wu and X. Ma, Preparation of multi-heteroatom self-doped carbon materials using industrial waste template agent combined with one-step carbonization: Multiple applications in supercapacitors and CO2 adsorption, *Sep. Purif. Technol.*, 2025, **373**, 133609.
43 A. Vinu, Two-Dimensional Hexagonally-Ordered Mesoporous Carbon Nitrides with Tunable Pore Diameter, Surface Area and Nitrogen Content, *Adv. Funct. Mater.*, 2008, **18**, 816–827.
44 Z. Y. Xu, L. R. Kong, H. Wang, Q. Ma, X. P. Shen, J. Y. Wang and S. Premlatha, Soft-template assisted preparation of

hierarchically porous graphitic carbon nitride layers for high-performance supercapacitors, *J. Appl. Polym. Sci.*, 2022, **139**, e52947.

45 M. B. Idris and S. Devaraj, Tuning the chemical composition, textural and capacitance properties of mesoporous graphitic carbon nitride, *Electrochim. Acta*, 2019, **303**, 219–230, DOI: 10.1016/j.electacta.2019.02.081.

46 L. Borchardt, M. Oschatz and S. Kaskel, Tailoring porosity in carbon materials for supercapacitor applications, *Mater. Horiz.*, 2014, **1**, 157–168.

47 M. B. Idris and S. Devaraj, Few-layered mesoporous graphitic carbon nitride: a graphene analogue with high capacitance properties, *New J. Chem.*, 2019, **43**, 11626–11635.

48 D. Leistenschneider, N. Jäckel, F. Hippauf, V. Presser and L. Borchardt, Mechanochemistry-assisted synthesis of hierarchical porous carbons applied as supercapacitors, *Beilstein J. Org. Chem.*, 2017, **13**, 1332–1341.

49 M. Jalalah, H. Han, A. K. Nayak and F. A. Harraz, High-performance supercapacitor based on self-heteroatom-doped porous carbon electrodes fabricated from Mikania micrantha, *Adv. Compos. Hybrid Mater.*, 2024, **7**, 20.

50 C. Kim, C. Zhu, Y. Aoki and H. Habazaki, Heteroatom-doped porous carbon with tunable pore structure and high specific surface area for high performance supercapacitors, *Electrochim. Acta*, 2019, **314**, 173–187.

51 E. Taer, A. Agustino, A. Fudholi, N. Chitraningrum and R. Taslim, High-performance symmetric supercapacitor based on activated carbon nanofibers derived from Napier grass fibers, *Diam. Relat. Mater.*, 2025, **155**, 112380.

52 Y. Wang, H. Wang, D. Zhu, Y. Xu, Z. Wang, Y. Li, Y. Tian and H. Lu, Micropore-dominant S, P co-doped carbon derived from biomass waste with rearranged pore structure for enhanced cycling stability supercapacitors, *J. Power Sources*, 2026, **667**, 239269.

53 T. Byambadorj, J. Zhang, Y. Li, F. Wang, Q. Liu and M. Chen, Advanced biomass-derived carbon materials for supercapacitors: fabrication methods, structure-property relationships, modifications, and prospects, *J. Electroanal. Chem.*, 2026, **1000**, 119573.

54 Z. Wu, J. Sun, P. Hu and W. Wang, Preparation of Biomass Carbon Materials and Their Several Typical Applications, in: *Biomass Based Prod.*, IntechOpen, 2024.

55 P. V. Vardhan, M. B. Idris, S. Manikandan, K. S. Rajan and S. Devaraj, Enhancement in the supercapacitive storage performance of $MnCO_3$ using SiO_x nanofluid-based electrolyte, *J. Solid State Electrochem.*, 2018, 1–6.

56 P. V. Vardhan, M. B. Idris, H. Y. Liu, S. R. Sivakkumar, P. Balaya and S. Devaraj, Tuning the Capacitance Properties of Nanocrystalline MnCO3 by the Effect of a Carbonizing Agent, *J. Electrochem. Soc.*, 2018, **165**, A1865–A1873.

57 M.-H. Kim, K.-B. Kim, S.-M. Park and K. C. Roh, Hierarchically structured activated carbon for ultracapacitors, *Sci. Rep.*, 2016, **6**, 21182.

58 S. Boonnun, P. Chaison, T. Meekati, C. Poochai, W. Pon-On, T. Amornsakchai and J. Sodtipinta, Biomass nanoarchitectonics of microporous activated carbon derived from gelatinized pineapple stem starch foam for high-performance supercapacitors, *J. Energy Storage*, 2025, **137**, 118554.

59 S. Balasubramaniam, A. Mohanty, S. K. Balasingam, S. J. Kim and A. Ramadoss, Comprehensive insight into the mechanism, material selection and performance evaluation of supercapatteries, *Nano-Micro Lett.*, 2020, **12**, 85.

60 J. Li, Z. Yu, X. Ma, X. Zhang and W. Yue, Co-pyrolysis of bamboo with low-dose guanidine phosphate to synthesis heteroatom-enriched porous carbon materials for supercapacitors, *J. Anal. Appl. Pyrolysis*, 2025, **189**, 107095.

61 M. B. Idris, B. B. Mamba and F. Xolile, Enhancing the energy density of phosphorus doped mesoporous carbon nitride using redox mediated gel-polymer electrolyte, *RSC Adv.*, 2025, **15**, 48762–48774.

62 A. A. Mirghni, M. J. Madito, T. M. Masikhwa, K. O. Oyedotun, A. Bello and N. Manyala, Hydrothermal synthesis of manganese phosphate/graphene foam composite for electrochemical supercapacitor applications, *J. Colloid Interface Sci.*, 2017, **494**, 325–337, DOI: 10.1016/j.jcis.2017.01.098.

63 T. Brousse, D. Bélanger and J. W. Long, To Be or Not To Be Pseudocapacitive?, *J. Electrochem. Soc.*, 2015, **162**, A5185, DOI: 10.1149/2.0201505jes.

64 M. D. Stoller and R. S. Ruoff, Best practice methods for determining an electrode material's performance for ultracapacitors, *Energy Environ. Sci.*, 2010, **3**, 1294–1301.

65 A. Noori, M. F. El-Kady, M. S. Rahmanifar, R. B. Kaner and M. F. Mousavi, Towards establishing standard performance metrics for batteries, supercapacitors and beyond, *Chem. Soc. Rev.*, 2019, **48**, 1272–1341.

66 S. G. Krishnan, H. T. A. Awan, M. Harilal, J. Alex, D. Sajan and M. Khalid, Rethinking Supercapacitors: A Guideline Perspective of Do's and Don'ts, *Battery Energy*, 2026, **5**, e70091.

67 A. A. Mirghni, M. J. Madito, K. O. Oyedotun, T. M. Masikhwa, N. M. Ndiaye, S. J. Ray and N. Manyala, A high energy density asymmetric supercapacitor utilizing a nickel phosphate/graphene foam composite as the cathode and carbonized iron cations adsorbed onto polyaniline as the anode, *RSC Adv.*, 2018, **8**, 11608–11621, DOI: 10.1039/C7RA12028A.

68 M. B. Idris, B. B. Mamba and F. Xolile, Polyvinyl alcohol and hydroquinone-based electrolyte coupled with mesoporous carbon nitride for high energy density supercapacitors, *RSC Adv.*, 2026, **16**, 953–966, DOI: 10.1039/D5RA08363J.

69 M. B. Idris, B. B. Mamba and F. Xolile, Construction of quasi-solid-state supercapacitor with enhanced high energy density based on carbon-rich graphitic carbon nitride and PVA-H2SO4 gel polymer electrolyte, *Diam. Relat. Mater.*, 2025, **160**, 113052, DOI: 10.1016/j.diamond.2025.113052.

70 P. Bharathidasan, M. B. Idris, D.-W. Kim, S. Sivakkumar and S. Devaraj, Exploiting the chemistry of redox active

compounds to enhance the capacitance of reduced graphene oxide, *FlatChem*, 2019, **15**, 100108.

71 E. S. Goda, S. E. Hong, B. Pandit, A. ur Rehman, B. S. Singu, M. S. Akhtar, M. Sohail, S. M. El-Bahy, H. Gamal and K. R. Yoon, Metal-organic framework (MOF) templated hierarchical Al-doped CoxP@ graphene composite: a promising solid-state asymmetric supercapacitor with PANI derived carbon nanorods, *J. Alloys Compd.*, 2023, **965**, 171183.

72 Y. Wang, X. Dong, Y. Xia, W. Wang, H. Song and S. Liu, High-performance nitrogen-doped porous carbon materials derived from waste biomass for supercapacitors, *Chem. Phys.*, 2025, **596**, 112745.

73 M. B. Idris and D. Sappani, Unveiling Mesoporous Graphitic Carbon Nitride as a High Performance Electrode Material for Supercapacitors (vol 3, pg 11258, 2018), *Chemistryselect*, 2019, **4**, 6886, DOI: 10.1002/slct.201902077.

74 S.-S. Wang, C.-H. Hsu, C.-T. Tsai, H.-P. Lin, C.-W. Yan, J.-K. Chang, T.-H. Hsieh, C.-W. Huang and C.-H. Lee, Conversion of wood waste into nitrogen-doped graphite-like multiporous carbon with high specific surface area and electrical conductivity for high-voltage supercapacitors, *Sustain. Energy Fuels*, 2025, **9**, 2355–2368, DOI: 10.1039/d4se01603c.

75 Md. Y. Bhat, F. Khan, Z. Ayoub, A. Jain and S. Gull, Recycling biowaste into energy storage: waste tea leaves-derived hierarchical porous activated carbon for supercapacitors, *J. Power Sources*, 2025, **655**, 237969.

76 Y. Ge, X. Xie, J. Roscher, R. Holze and Q. Qu, How to measure and report the capacity of electrochemical double layers, supercapacitors, and their electrode materials, *J. Solid State Electrochem.*, 2020, **24**, 3215–3230, DOI: 10.1007/s10008-020-04804-x.

77 N. Rawat, S. Kathuria, S. Kumar, S. Nazir, P. Joshi, P. K. Singh, F. M. Hamzah, M. Diantoro, V. D. Punetha and P. S. Dhapola, Microporous activated carbon derived from Murraya Koenigii seeds for high-performance supercapacitors, *Ionics*, 2025, **31**, 3727–3744, DOI: 10.1007/s11581-025-06159-7.

78 P. Taberna, P. Simon and J.-F. Fauvarque, Electrochemical characteristics and impedance spectroscopy studies of carbon-carbon supercapacitors, *J. Electrochem. Soc.*, 2003, **150**, A292–A300.

79 D. I. Abouelamaiem, G. He, T. P. Neville, D. Patel, S. Ji, R. Wang, I. P. Parkin, A. B. Jorge, M.-M. Titirici and P. R. Shearing, Correlating electrochemical impedance with hierarchical structure for porous carbon-based supercapacitors using a truncated transmission line model, *Electrochim. Acta*, 2018, **284**, 597–608.

80 K. Panchal, K. Bhakar, K. S. Sharma, D. Kumar and S. Prasad, Review on electrochemical impedance spectroscopy: a technique applied to hollow structured materials for supercapacitor and sensing applications, *Appl. Spectrosc. Rev.*, 2025, **60**, 30–55.

81 P. V. Vardhan, M. B. Idris, V. Ramanathan and S. Devaraj, Electrodeposited MnCO3 as a High Performance Electrode Material for Supercapacitor, *Chemistryselect*, 2018, **3**, 6775–6778.

82 J. Xu, N. Yang, S. Yu, A. Schulte, H. Schönherr and X. Jiang, Ultra-high energy density supercapacitors using a nickel phosphide/nickel/titanium carbide nanocomposite capacitor electrode, *Nanoscale*, 2020, **12**, 13618–13625, DOI: 10.1039/D0NR01984D.

83 H. Li, C. Qi, Y. Tao, H. Liu, D. Wang, F. Li, Q. Yang and H. Cheng, Quantifying the volumetric performance metrics of supercapacitors, *Adv. Energy Mater.*, 2019, **9**, 1900079.

84 E. E. Mathew and M. Balachandran, Evaluating the electrochemical performance of single and multiple heteroatom doped carbon black from waste tires for supercapacitor application, *J. Power Sources*, 2025, **659**, 238437.

85 Y. Gogotsi and P. Simon, True performance metrics in electrochemical energy storage, *Science*, 2011, **334**, 917–918.

86 Q. Wang, J. Yan and Z. Fan, Carbon materials for high volumetric performance supercapacitors: design, progress, challenges and opportunities, *Energy Environ. Sci.*, 2016, **9**, 729–762.

87 M. O. Bamgbopa, D. Belaineh, D. A. Mengistie, J. Edberg, I. Engquist, M. Berggren and K. Tybrandt, Modelling of heterogeneous ion transport in conducting polymer supercapacitors, *J. Mater. Chem. A*, 2021, **9**, 2184–2194.

88 H. Li, G. Bucci, N. W. Brady, N. R. Cross, V. M. Ehlinger, T. Y. Lin, M. Salazar de Troya, D. Tortorelli, M. A. Worsley and T. Roy, Topology optimization for the full-cell design of porous electrodes in electrochemical energy storage devices, *Struct. Multidiscip. Optim.*, 2024, **67**, 188.

89 A. Neumann, S. Randau, K. Becker-Steinberger, T. Danner, S. Hein, Z. Ning, J. Marrow, F. H. Richter, J. Janek and A. Latz, Analysis of interfacial effects in all-solid-state batteries with thiophosphate solid electrolytes, *ACS Appl. Mater. Interfaces*, 2020, **12**, 9277–9291.

90 T. R. Garrick, B. J. Koch, J. Gao, A. Zhang and J. S. Lowe, Modeling Losses in a Three Electrode System Towards Fast Charge Control, *J. Electrochem. Soc.*, 2025, **172**, 043511.

91 K. Xu, S. P. Ding and T. R. Jow, Toward reliable values of electrochemical stability limits for electrolytes, *J. Electrochem. Soc.*, 1999, **146**, 4172–4178.

92 R. Dugas, Y. Dupraz, E. Quemin, T. Koç and J.-M. Tarascon, Engineered three-electrode cells for improving solid state batteries, *J. Electrochem. Soc.*, 2021, **168**, 090508.

93 Z. Bian, C. Wu, C. Yuan, Y. Wang, G. Zhao, H. Wang, Y. Xie, C. Wang, G. Zhu and C. Chen, One-step production of N–O–P–S co-doped porous carbon from bean worms for supercapacitors with high performance, *RSC Adv.*, 2020, **10**, 30756–30766.

94 J. W. Jeon, J. Shin, J. Lee, J.-H. Baik, R. Malpass-Evans, N. B. McKeown, T.-H. Kim, J.-C. Lee, S.-K. Kim and B. G. Kim, Hierarchically structured carbon electrodes derived from intrinsically microporous Tröger's base polymers for high-performance supercapacitors, *Appl. Surf. Sci.*, 2020, **530**, 147146.

95 S. A. Ageeb, A. Alrubayyi, L. M. Mokhtar, A. Q. Alshammari, I. A. Salim and H. A. Hamouda, Synthesis of Nitrogen-Doped Activated Carbon Nanosheets Based on Biomass Derived from Waste Wheat Husks for Energy Storage, *ChemistrySelect*, 2025, **10**, e04548.
96 J. Lei, Y. Zhang, X. Ren, Q. He and S. Wang, Porous carbon derived from vinegar residue as a typical waste utilization for supercapacitors, *Diam. Relat. Mater.*, 2025, **156**, 112434.
97 E. Taer, A. Apriwandi, A. Fudholi, N. Chitraningrum and R. Taslim, Turnip-waste derived nanoarchitectonic engineering and multi-heteroatom doping carbon for advanced EDL-supercapacitors, *Phys. Scr.*, 2025, **100**, 085959.
98 Y. Wu, X.-Y. Cui, L. Pan, R. Li, Y.-X. Li, H.-X. Fang, Y. Wang, M.-H. Ge and Q.-Q. Zhuang, Oxygen-Enriched Porous Carbon Derived from Biomass Waste for Supercapacitors with High Electrochemical Performances, *Energy Technol.*, 2025, **13**, 2500429.
99 K. N. R. Stulasti, L. F. Aziz, A. Jamaluddin, S. Widiyastuti, R. T. Subramaniam and A. Purwanto, Engineering optimization of tea waste-derived activated carbon/graphite composites for supercapacitors, *Results Eng.*, 2026, **29**, 109191.
100 D. S. Rana, R. Sharma, A. Awasthi, D. Singh and A. Sharma, Boron-doped biomass-derived nanocarbon for efficient supercapacitors: bridging waste recycling and energy storage, *New J. Chem.*, 2025, **49**, 13726–13737, DOI: 10.1039/d5nj01732g.
101 X. Tang, Q. Tang, J. Hou, Y. Li, J. Sun, Y. Xie, L. Xiao and X. Fan, Bamboo waste-derived N, P co-doped hierarchical porous carbon for high-performance energy storage, *J. Power Sources*, 2025, **647**, 237356.
102 C. Xu, X. Liang, Q. He, Z. Zhou, X. Fan, H. Zhan, Y. Zheng, W. Tang, Y. Wang, W. Zhang, L. Leng and H. Li, Molten salt-mediated carbonization-activation of waste wood-based panels toward nitrogen-doped porous carbon for supercapacitors: Synergistic nitrogen self-doping and pore engineering, *J. Energy Storage*, 2026, **153**, 120951.
103 N. Dhanavel, G. B. Chavati, S. K. Basavaraju, M. B. Sannaobaiah, R. Viswanatha, K. Venkatesh and H. B. Muralidhara, Coconut bract derived activated carbon: a good performance material for supercapacitors, *Emergent Mater.*, 2025, **8**, 5545–5555, DOI: 10.1007/s42247-025-01202-9.
104 T. Yang, T. Ma, P. Yuan, J. Xiang, H. Zheng, L. Yang, J. Wei, H. Xue, K. Cheng, Z. Fang and J. Ye, Biomass-derived porous carbon from waste broad bean husk for high-performance all-solid-state supercapacitors, *Diam. Relat. Mater.*, 2025, **160**, 113000.
105 D. Hu, N. He, H. Xie, Z. Wu, Z. Wang, R. Zhu, K. Wang, H. Pan, Z. Chen and Q. Lin, Tailoring waste sawdust-derived porous carbon through varying glycosidic bond cleavage: Analysis of pore structure mechanism and applications in supercapacitors and dye removal, *J. Anal. Appl. Pyrolysis*, 2025, **191**, 107178.
106 T. Liu, Y. Liu, F. Zhou, W. Chen, X. Zhao, X. Li and X. Su, Chemical exfoliation synthesis of N, O-doped tea Saponin-derived carbon for high-performance electrochemical electrodes, *Diam. Relat. Mater.*, 2025, **156**, 112401.
107 J. Zheng, T. Cao, B. Ding, X. Zhang, H. Wu and X. Li, Facile synthesis of N, P co-doped carbon materials derived from corn bract for high-performance symmetric supercapacitors, *J. Energy Storage*, 2025, **110**, 115297.
108 K. D. Verma and K. K. Kar, Melanin-driven heteroatom incorporation in bird feather-derived activated carbon for high-performance supercapacitors, *J. Electroanal. Chem.*, 2026, **1003**, 119777.
109 W. Jin, W. Li, R. Sun, X. Zhang, M. Wu, H. S. Haider, D. Ma, Y. Ma and L. Ma, High-performance flexible supercapacitors based on porous carbon derived from Setaria viridis stalks, *J. Indian Chem. Soc.*, 2025, **102**, 102074.
110 A. Rao, S. Bhat, S. De, A. Rag and V. Cyriac, From steel waste to energy storage: kish graphite derived graphene electrodes for high performance supercapacitors, *Mater. Adv.*, 2025, **6**, 5486–5505, DOI: 10.1039/d5ma00399g.
111 P. Atanasio, R. Y. S. Zampiva, A. Fornari, C. Mancini, A. Aurora, A. G. Marrani, M. Rossi, M. Pasquali and F. A. Scaramuzzo, Green synthesis of carbon aerogels derived from rice husk for advanced supercapacitors, *J. Energy Storage*, 2025, **116**, 115901.
112 J. Yin, Y. Guo, K. Yan, Y. Sun, Y. Chen and J. Pan, Hierarchical porous carbon from waste tire pyrolysis carbon black *via in situ* SiO_2 templating for high-performance supercapacitors, *J. Power Sources*, 2026, **661**, 238603.
113 P. Yuan, T. Ma, J. Xiang, T. Yang, H. Zheng, Z. Wang, L. Yang, J. Wei, H. Xue, K. Cheng, Z. Fang and J. Ye, Waste chrysanthemum stem derived honeycomb like porous carbon materials for fabricating high performance flexible all solid state supercapacitors, *J. Energy Storage*, 2026, **146**, 120111.
114 F. Ma and H. Zhao, Preparation and Capacitive Performance of Nitrogen-Doped Natural Integrated Carbon Sheets Derived From Waste Leather, *Energy Technol.*, 2026, **14**, e202501688.
115 V. K. Kumar, S. C. Hallad and N. L. Panwar, Development of carbon electrodes and electrochemical double-layer supercapacitors using agricultural crop residue biomass-derived porous carbon, *Clean Energy*, 2026, **10**, 15–28, DOI: 10.1093/ce/zkaf057.
116 R. Yan, M. Antonietti and M. Oschatz, Toward the experimental understanding of the energy storage mechanism and ion dynamics in ionic liquid based supercapacitors, *Adv. Energy Mater.*, 2018, **8**, 1800026.
117 A. C. Forse, J. M. Griffin, C. Merlet, J. Carretero-Gonzalez, A.-R. O. Raji, N. M. Trease and C. P. Grey, Direct observation of ion dynamics in supercapacitor electrodes using *in situ* diffusion NMR spectroscopy, *Nat. Energy*, 2017, **2**, 16216.
118 D. T. Galhena, B. C. Bayer, S. Hofmann and G. A. Amaratunga, Understanding capacitance variation

in sub-nanometer pores by *in situ* tuning of interlayer constrictions, *ACS Nano*, 2016, **10**, 747–754.

119 N. Jackel, P. Simon, Y. Gogotsi and V. Presser, Increase in capacitance by subnanometer pores in carbon, *ACS Energy Lett.*, 2016, **1**, 1262–1265.

120 C. O. Ania, J. Pernak, F. Stefaniak, E. Raymundo-Piñero and F. Béguin, Polarization-induced distortion of ions in the pores of carbon electrodes for electrochemical capacitors, *Carbon*, 2009, **47**, 3158–3166.

121 B. Pal, S. Yang, S. Ramesh, V. Thangadurai and R. Jose, Electrolyte selection for supercapacitive devices: a critical review, *Nanoscale Adv.*, 2019, **1**, 3807–3835.

122 H. Shao, Y.-C. Wu, Z. Lin, P.-L. Taberna and P. Simon, Nanoporous carbon for electrochemical capacitive energy storage, *Chem. Soc. Rev.*, 2020, **49**, 3005–3039.

123 M. B. Idris and D. Sappani, Unveiling Mesoporous Graphitic Carbon Nitride as a High Performance Electrode Material for Supercapacitors, *Chemistryselect*, 2018, **3**, 11258–11269.

124 S. Bonyadi, K. Ghanbari and M. Ghiasi, All-electrochemical synthesis of a three-dimensional mesoporous polymeric g-C_3N_4/PANI/CdO nanocomposite and its application as a novel sensor for the simultaneous determination of epinephrine, paracetamol, mefenamic acid, and ciprofloxacin, *New J. Chem.*, 2020, **44**, 3412–3424, DOI: 10.1039/c9nj05954g.

125 T. Liu, Z. Zhou, Y. Guo, D. Guo and G. Liu, Block copolymer derived uniform mesopores enable ultrafast electron and ion transport at high mass loadings, *Nat. Commun.*, 2019, **10**, 675.

126 J. F. Gabitto and C. Tsouris, A review of transport models in charged porous electrodes, *Front. Chem. Eng.*, 2023, **4**, 1051594.

127 L. Borchardt, D. Leistenschneider, J. Haase and M. Dvoyashkin, Revising the concept of pore hierarchy for ionic transport in carbon materials for supercapacitors, *Adv. Energy Mater.*, 2018, **8**, 1800892.

128 M. B. Idris, G. H. Sai, D. Hemalatha, G. Sakthivel and S. Devaraj, The Effect of Phosphorous Doping on the Composition and Capacitance Properties of Mesoporous Graphitic Carbon Nitride, *J. Electrochem. Soc.*, 2019, **166**, A2409–A2418, DOI: 10.1149/2.0311912jes.

129 P. Bharathidasan, M. B. Idris, D.-W. Kim, S. R. Sivakkumar and S. Devaraj, Enhanced capacitance properties of nitrogen doped reduced graphene oxide obtained by simultaneous reduction and nitrogen doping, *FlatChem*, 2018, **11**, 24–31, DOI: 10.1016/j.flatc.2018.10.001.

130 G. Hasegawa, T. Deguchi, K. Kanamori, Y. Kobayashi, H. Kageyama, T. Abe and K. Nakanishi, High-level doping of nitrogen, phosphorus, and sulfur into activated carbon monoliths and their electrochemical capacitances, *Chem. Mater.*, 2015, **27**, 4703–4712.

131 L. Shabnam, S. N. Faisal, A. Martucci and V. G. Gomes, Doping reduced graphene oxide and graphitic carbon nitride hybrid for dual functionality: High performance supercapacitance and hydrogen evolution reaction, *J. Electroanal. Chem.*, 2020, **856**, 113503.

132 L. Xie, F. Su, L. Xie, X. Guo, Z. Wang, Q. Kong, G. Sun, A. Ahmad, X. Li and Z. Yi, Effect of pore structure and doping species on charge storage mechanisms in porous carbon-based supercapacitors, *Mater. Chem. Front.*, 2020, **4**, 2610–2634.

133 Y. Wang, H. Wang, D. Zhu, Y. Xu, Z. Wang, Y. Li, Y. Tian and H. Lu, Micropore-dominant S, P co-doped carbon derived from biomass waste with rearranged pore structure for enhanced cycling stability supercapacitors, *J. Power Sources*, 2026, **667**, 239269.

134 Z. Zhao, H. Chen, W. Zhang, S. Yi, H. Chen, Z. Su, B. Niu, Y. Zhang and D. Long, Defect engineering in carbon materials for electrochemical energy storage and catalytic conversion, *Mater. Adv.*, 2023, **4**, 835–867.

135 C. Arbizzani, Good practice guide for papers on supercapacitors and related hybrid capacitors for the Journal of Power Sources, *J. Power Sources*, 2020.

136 A. Dahiru Shuaibu, A. Saeed Alzahrani and M. A. Aziz, High-performance Supercapacitors Enabled by Highly-porous Date Stone-derived Activated Carbon and Organic Redox Gel Electrolyte, *Asian J. Org. Chem.*, 2023, **12**, e202300050.

137 B. Abubakar Abdulkadir and H. D. Setiabudi, Progress and Accomplishments in Polymer Blend Electrolytes for Electrochemical Energy Storage: A Comprehensive Review, *Polym.-Plast. Technol. Mater.*, 2025, 1–36.